Soil Dynamics and Earthquake Engineering xxx (xxxx) xxx–xxx

Contents lists available at ScienceDirect

Soil Dynamics and Earthquake Engineering

journal homepage: www.elsevier.com/locate/soildyn

Liquefaction experiment and analysis projects (LEAP): Summary of observations from the planning phase

Majid T. Manzari[a,*], Mohamed El Ghoraiby[a], Bruce L. Kutter[b], Mourad Zeghal[c], Tarek Abdoun[c], Pedro Arduino[d], Richard J. Armstrong[e], Michael Beaty[f], Trevor Carey[b], Yunmin Chen[g], Alborz Ghofrani[d], David Gutierrez[h], Nithyagopal Goswami[c], Stuart K. Haigh[i], Wen-Yi Hung[j], Susumu Iai[k], Panagiota Kokkali[c], Chung-Jung Lee[j], S.P. Gopal Madabhushi[i], Lelio Mejia[l], Michael Sharp[m], Tetsuo Tobita[n], Kyohei Ueda[k], Yanguo Zhou[g], Katerina Ziotopoulou[b]

[a] Department of Civil and Environmental Engineering, George Washington University, Washington, D.C., USA
[b] Department of Civil and Environmental Engineering, University of California, Davis, USA
[c] Department of Civil and Environmental Engineering, Rensselaer Polytechnic Institute, Troy, NY, USA
[d] Department of Civil and Environmental Engineering, University of Washington, Seattle, USA
[e] Department of Civil and Environmental Engineering, California State University, Sacramento, USA
[f] Beaty Engineering LLC, USA
[g] Department of Civil and Environmental Engineering, Zhejiang University, Hangzhou, Zhejiang, China
[h] GEI Consultants, Inc., Formerly at Division of Safety of Dams, Sacramento, CA, USA
[i] Geosyntec Consultants, 1111 Broadway, 6th Floor, Oakland, CA 94607, USA
[j] Department of Civil Engineering, National Central University of Taiwan, Taoyuan City, Taiwan
[k] Disaster Prevention Research Institute, Kyoto University, Kyoto, Japan
[l] AECOM Corp., Oakland, CA, USA
[m] US Army Corps of Engineers, MS, USA
[n] Department of Civil, Environmental and Applied System Engineering, Kansai University, Osaka, Japan

ARTICLE INFO

Keywords:
Calibration
Centrifuge modeling
Constitutive modeling
Elastoplasticity
Liquefaction
Numerical modeling
Validation

ABSTRACT

The LEAP international collaboratory is introduced and its key objectives and main accomplishments during the planning phase of the US-LEAP (LEAP-2015) are presented. The main theme of LEAP-2015 was lateral spreading of sloping liquefiable soils. A summary of the results of the laboratory element tests performed on the selected soil (Ottawa F-65) is presented. The numerical simulations submitted by several predictors at different stages of the project are compared with the measured responses of sloping deposit specimens tested in a rigid box at six different centrifuge facilities around the world. The comparisons are presented for three rounds of simulations labeled here as types A, B, and C simulations. The type A simulations involved the response of the soil specimen to a prescribed base excitation with a maximum amplitude of 0.15*g* (Motion #2). Comparisons of the numerical simulations with the experimental results show that a sub-set of type A simulations were in reasonably good agreement with the responses measured in the reference centrifuge experiment. The predictors subsequently assessed the performance of their type A simulations by comparing them to the measured responses, made the necessary adjustments in their models, and conducted a type B simulation of the response of the same soil specimen subjected to an amplified base excitation with a maximum amplitude of 0.25*g* (Motion #4). In these type B simulations, the achieved base motions were used and the simulations showed an improved correlation with the experimental results. The predictors also conducted a type C simulation of the original test (Motion #2) using the base motions achieved on the six centrifuge facilities. The results showed very good agreement with the experimental results.

1. Introduction

Liquefaction-induced permanent deformations and failure in geo-structures such as retaining structures, soil slopes, and earth embankments remain a major concern to the geotechnical engineering community. Following large earthquakes, recorded data,

* Corresponding author.
E-mail address: manzari@gwu.edu (M.T. Manzari).

http://dx.doi.org/10.1016/j.soildyn.2017.05.015
Received 21 September 2016; Received in revised form 3 April 2017; Accepted 8 May 2017

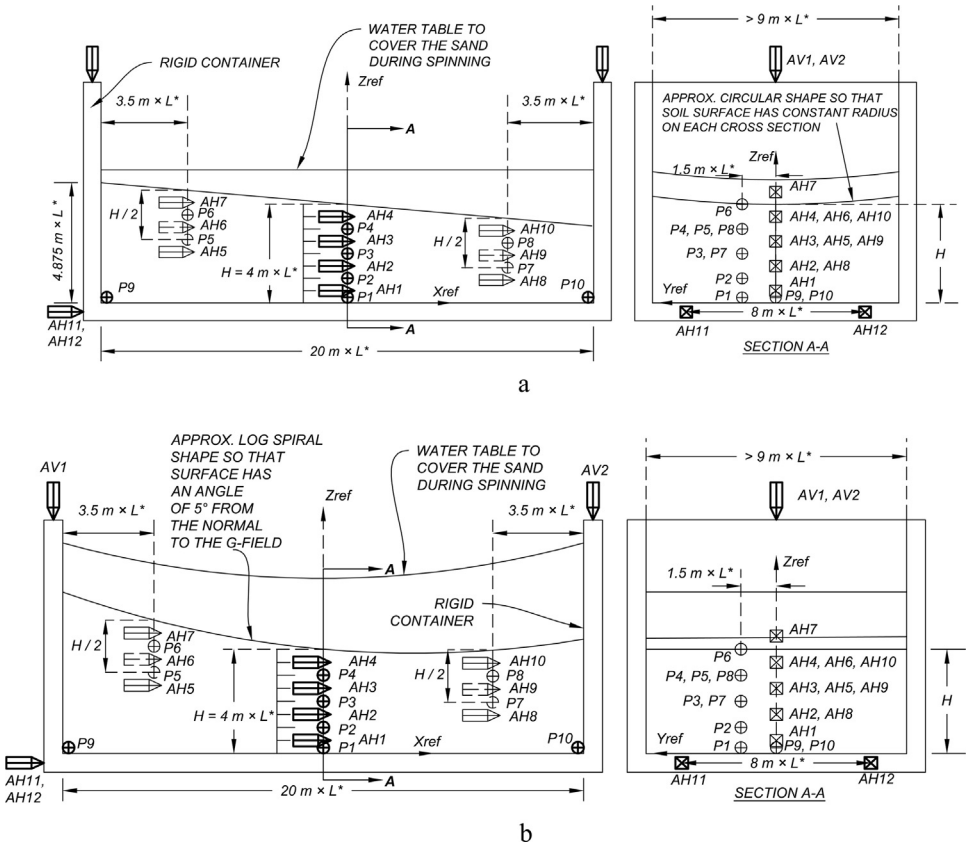

Fig. 1. a: Schematic for GWU 2015 validation experiment for shaking parallel to the axis of the centrifuge. b: Schematic for GWU 2015 validation experiment for shaking in the plane of spinning the centrifuge.

Table 1
Participating centrifuge facilities [35].

Symbol	Facility	Centrifuge Radius (m)	g*	Shaking direction	Density of soil (kg/m^3)
CU	Cambridge University	4.0	40.0	Tangential	1620 ± 20
KU	Kyoto University	2.5	44.4	Tangential	1652
NCU	National Central University of Taiwan	3.0	26.0	Axial	1648
RPI	Rensselaer Polytechnic Institute	3.0	23.0	Axial	1650
UCD	University of California at Davis	1.0	43.0	Tangential	1652 ± 10
ZJU	Zhejiang University	4.5	26.0	Axial	1644 ± 54

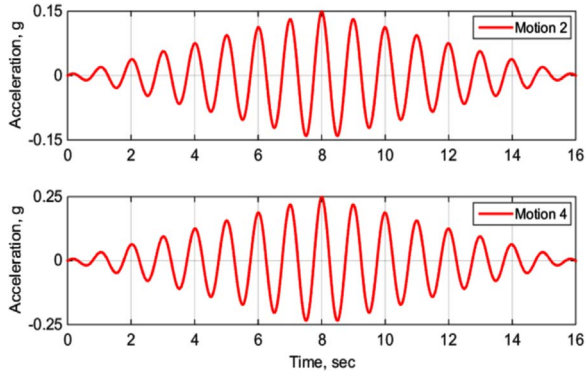

Fig. 2. Target base motions for Events 2 and 4.

field investigations, and various case studies have often been used to understand the mechanisms of failure and to establish a link to key features of soil stress-strain-strength behavior. Furthermore, intensive efforts have been undertaken by researchers towards the development of constitutive and numerical modeling tools capable of predicting cyclic and permanent deformations of liquefaction prone soils (e.g., [26,38,67,20,17,31,27,28]). Except for occasional efforts such as that by EPRI (1993), thorough assessments and validations of these computational tools have been rather limited. Perlea and Beaty [47] have discussed the use of three different codes including FLAC (with a hypoplasticity model, Wang et al., 2006; with UBCSand model, [9]; and with an empirical pore pressure generation model, [18]), DYNAFLOW [48], and TARA [23] in the assessment of the seismic response of a number of earth dams. Boulanger and Ziotopoulou [12], in the framework of the constitutive model's PM4Sand development, presented an extensive

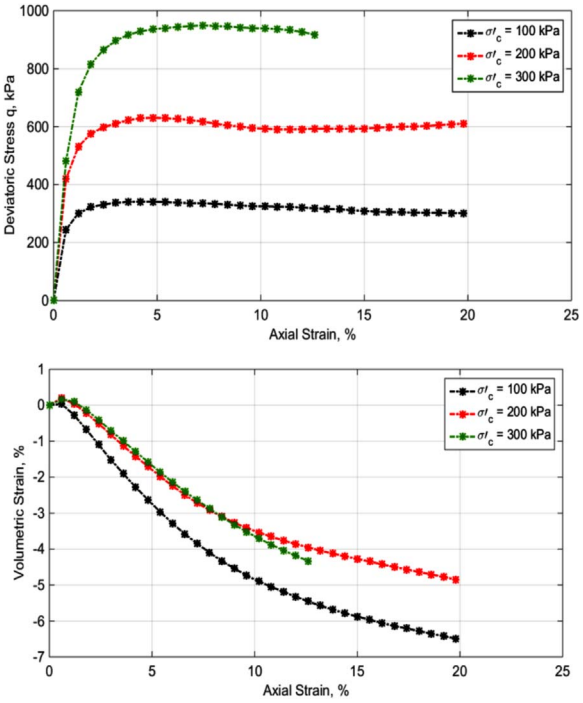

Fig. 3. Results of three monotonic drained compression tests conducted on Ottawa sand with initial dry density of 1657 kg/m^3 (σ_c = 100 kPa), 1659 kg/m^3 (σ_c = 200 kPa), 1662 (σ_c = 300 kPa) kg/m^3 [54].

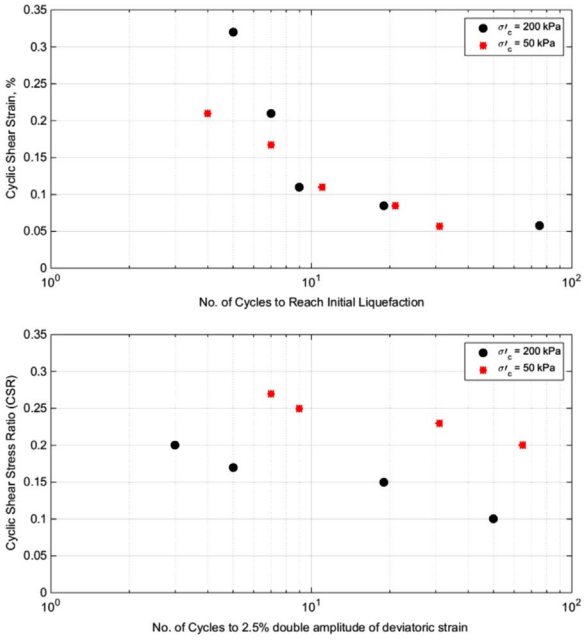

Fig. 4. Results of strain-controlled and stress-controlled cyclic undrained tests conducted on Ottawa sand with an average initial density of 1658 kg/m^3 and a coefficient of variation of 0.134% [54].

validation of single-element simulations against the body of data available for liquefiable soils and demonstrated capabilities and limitations of their constitutive model. The extensive computational work reported in Perlea and Beatty [47] and Boulanger and Ziotopoulou [12] clearly demonstrates the continuing need of practicing engineers for validation and assessment of modern numerical tools that are now available for geotechnical analysis.

In the early 1990's, over 20 teams of numerical modelers participated in an elaborate prediction exercise called VELACS (VErification Liquefaction Analyses by Centrifuge Studies) [4]. Centrifuge tests were conducted and duplicated at different centrifuge facilities in the US (UCD, RPI, University of Colorado at Boulder, and Princeton University) and Cambridge University in the UK. A large number of "Class A" (i.e., true prediction of an event made prior to the event, hereafter referred to as TP) numerical simulations of these centrifuge tests were submitted and compared at a symposium. The two key lessons learned from this exercise were that: (1) none of the numerical techniques available at that time were reliable for producing high quality predictions of liquefaction problems, and (2) there was significant variability in many of the centrifuge test results.

Over the past few decades, the geotechnical engineering community has seen remarkable advances in experimental and computational simulation capabilities [1, 2, 21, 51]. Experimental research using increasingly reliable element scale laboratory tests, in-situ tests, and centrifuge experiments have provided the community with significantly improved understanding of the response of geosystems to earthquake loading.

In the same vein as the VELACS project, a recent exercise was conducted in Italy, on predicting the tunnel-soil interaction using numerical procedures that are matched to centrifuge test data. This project titled Round Robin Tunnel Tests (RRTT) has involved seven different numerical modeling teams that were involved in predicting the centrifuge test results in terms of tunnel lining forces and bending moments amongst other parameters, Bilotta et al. [6].

The tremendous advances in computational power and computational methods currently provide an unprecedented opportunity for the analysis of very large geo-structural systems using sophisticated constitutive and numerical modeling techniques. Compared to 25 years ago, there are far better computational and numerical modeling techniques available for the analysis of soil liquefaction and its consequences. In the realm of constitutive modeling, there are several well-established constitutive models for saturated granular soils [8–12,16,17,19,20,26–28,36,38,46,50,55–60]. Moreover, several commercial finite element and finite difference codes [e.g., PLAXIS [7]; FLAC [30]] provide nonlinear fully-coupled effective stress capabilities for analysis of geostructures involving liquefiable soils. New advances in meshfree [41], finite element analysis [39,41,42,43–45,49] and discrete element techniques [22,61,63] have provided the community with powerful

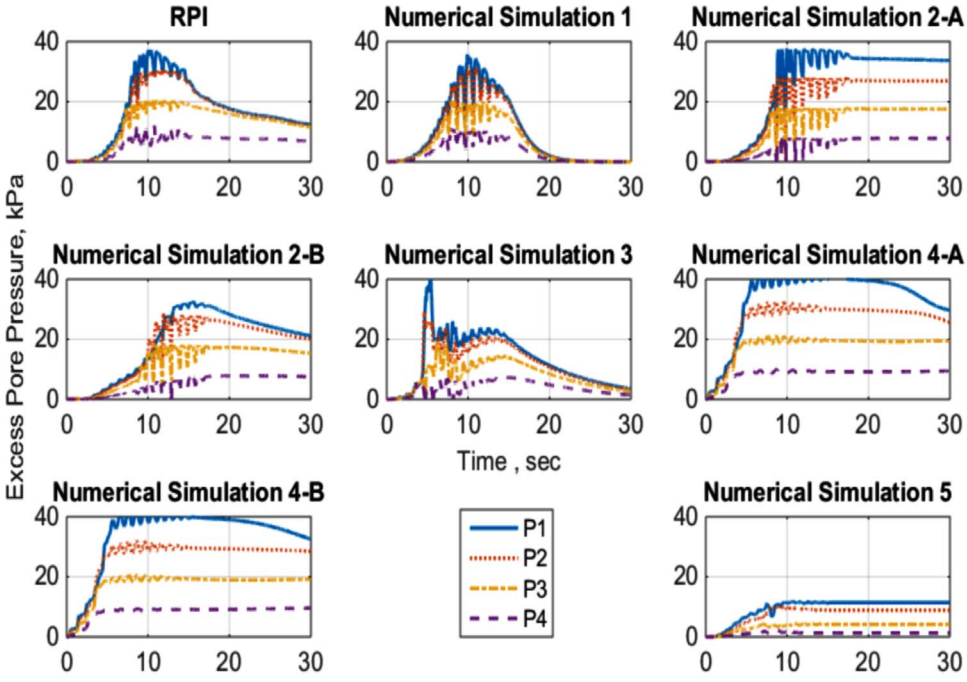

Fig. 5. Comparison of type A simulations of the excess pore water pressure time histories at the location of P1, P2, P3, and P4 with the results of the reference experiment, Motion #2 (see Fig. 1 for transducer locations.).

RMSE-t16

	P1	P2	P3	P4
NS 1	0.1179	0.1494	0.1380	0.1878
NS 2-A	0.1175	0.1331	0.1965	0.2496
NS 2-B	0.2522	0.2546	0.2753	0.3205
NS 3	0.2811	0.3258	0.2933	0.2676
NS 4-A	0.3892	0.3923	0.3725	0.3751
NS 4-B	0.3814	0.3834	0.3645	0.3622
NS 5	0.3617	0.4436	0.5434	0.5047

RMSE-t30

	P1	P2	P3	P4
NS 1	0.2571	0.3356	0.4565	0.4783
NS 2-A	0.3177	0.2719	0.1851	0.1853
NS 2-B	0.2469	0.2539	0.2180	0.2361
NS 3	0.2422	0.2953	0.3492	0.3366
NS 4-A	0.4474	0.4106	0.3209	0.2980
NS 4-B	0.4508	0.4108	0.3105	0.2906
NS 5	0.2812	0.3669	0.5364	0.5634

tools to model liquefaction as well as post-failure response of geo-structures.

All these advanced computational tools still need to be assessed and validated against high-fidelity experiments. This paper presents the results of the preliminary experimental and numerical simulations performed by a group of researchers as part of an international collaborative LEAP effort [33,34,40,62].

2. Design of GWU 2015 validation experiment

A key objective of LEAP is to develop a database of high quality centrifuge tests that can be used to assess the validity of current and future constitutive/numerical modeling techniques for the analysis of soil liquefaction and its consequences such as permanent deformation. Earthquake-induced lateral spreading was selected as a topic of interest in the planning phase of the US project. A recent study of the centrifuge [64] showed that laminar box used in centrifuge modeling of lateral spreading caused by soil liquefaction may influence the data (especially at high pore pressure ratios).

The LEAP-2015 model is composed of uniform sand, with a 5-degree slope instrumented as shown in shown in Fig. 1a and b (see [35] for more details). The experiment was designed to be both repeatable at all six of the centrifuge facilities (Table 1). Some centrifuge facilities have hydraulic shakers that produce 1-D horizontal shaking in the plane of spinning, while other facilities perform the shaking along the axis of the centrifuge. To account for the differences in orientation of the shaking direction in the radial acceleration field, the 5 degree slope in the shaking direction is to be superimposed on a curved surface corresponding to the radius from the axis of rotation of the centrifuge. If the surface was not curved initially, it would become curved to some extent as a result of liquefaction; settlements associated with the forming of the curve

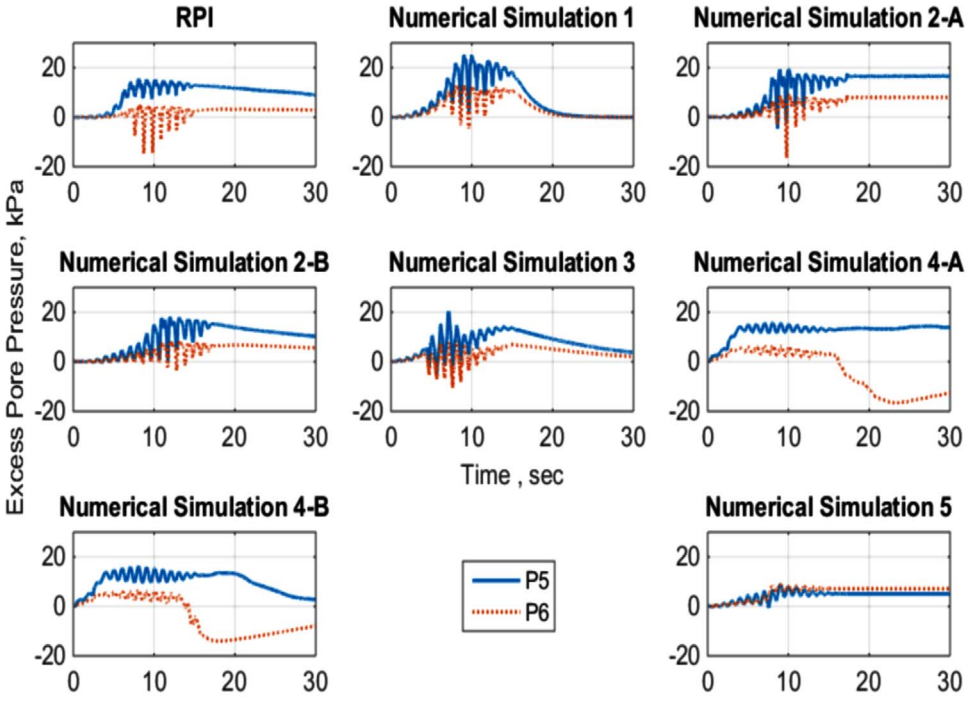

Fig. 6. Comparison of type A simulations of excess pore water pressure time histories at the location of P5 and P6 with the results of the reference experiment, Motion #2 (see Fig. 1 for transducer locations.).

RMSE-t16

	P5	P6
NS 1	0.2322	0.6656
NS 2-A	0.1645	0.3572
NS 2-B	0.2062	0.3510
NS 3	0.1555	0.3669
NS 4-A	0.2656	0.3831
NS 4-B	0.2479	0.4944
NS 5	0.2915	0.5069

RMSE-t30

	P5	P6
NS 1	0.3528	0.5178
NS 2-A	0.2251	0.4185
NS 2-B	0.1634	0.3381
NS 3	0.1713	0.2906
NS 4-A	0.2198	1.1198
NS 4-B	0.2217	1.0609
NS 5	0.2928	0.4607

would be superimposed on settlements due to consolidation and spreading down the 5 degree slope. The surface curvature is important to minimize differences between experiments at different facilities.

The centrifuge experiments consist of five shaking events. During these events the centrifuge specimen is subjected to a tapered sinusoidal motion. Events 2 and 4 are the main events, while events 1, 3 and 5 consist of non-destructive base excitations. Fig. 2 shows the target base motions for the main events of the centrifuge experiments. Motions 2 and 4 have peak acceleration of 0.15*g* and 0.25*g* respectively.

In prototype scale, the slope is 20 m in length and 4 m deep at the midpoint. The width of the cross section, shown as section A-A in Figs. 1 and 2 was specified to be at least 9 m to control boundary effects produced by friction on the sidewalls of the container. The model-scale dimensions are specific to each centrifuge facility, largely determined by the available rigid model containers.

The locations of the accelerometers and pore pressure transducers are specified in Figs. 1 and 2. Required sensors shown in bold, highly recommended sensors are shown in bold dashed lines, and recommended sensors are shown as non-bolded solid line symbols in Figs. 1 and 2.

Required sensors include AH11 and AH12 to measure the achieved base motion and are spaced consistently such that the yaw rotational acceleration can be determined. The vertical accelerometers, AV1 and AV2 are sensitive to container due to the rocking and Coriolis accelerations which depend on the shaking direction. The central vertical array (P1-P4 and AH1-AH4) were

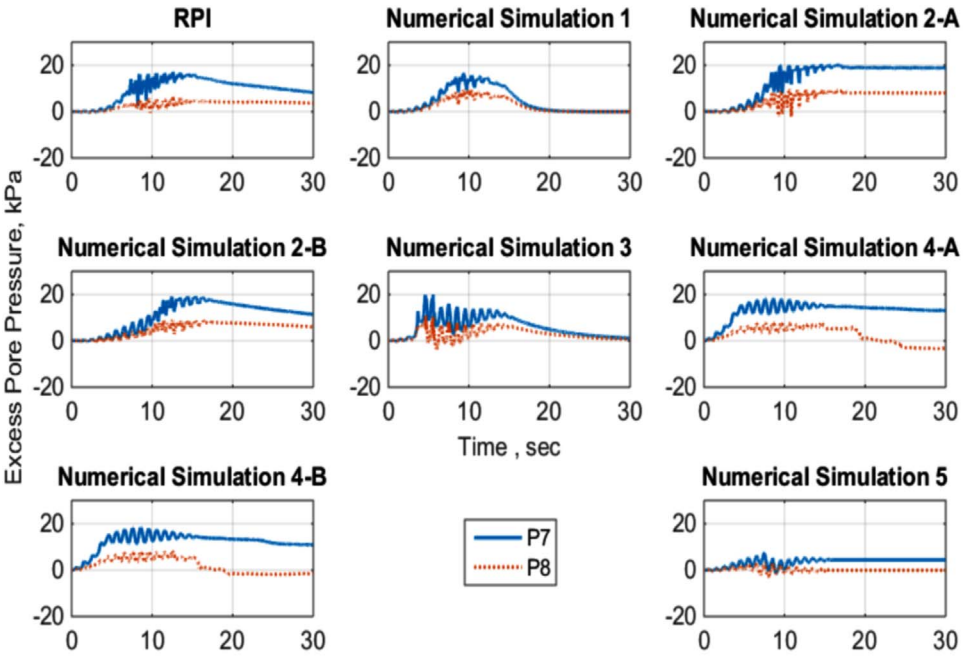

Fig. 7. Comparison of type A simulations of excess pore water pressure time histories computed at the location of P7 and P8 with the results of the reference experiment, Motion #2 (see Fig. 1 for transducer locations.).

RMSE-t16

	P7	P8
NS 1	0.1494	0.2654
NS 2-A	0.1338	0.2641
NS 2-B	0.1467	0.1994
NS 3	0.2559	0.2665
NS 4-A	0.2847	0.2796
NS 4-B	0.2821	0.2765
NS 5	0.3862	0.2860

RMSE-t30

	P7	P8
NS 1	0.3691	0.3183
NS 2-A	0.2903	0.3348
NS 2-B	0.1587	0.2598
NS 3	0.3102	0.2432
NS 4-A	0.2331	0.4009
NS 4-B	0.2133	0.4135
NS 5	0.3665	0.3524

located to minimize the boundary effects from the rigid walls [65]. The pore pressure transducers and accelerometers are offset 1.5 m in the transverse direction (section A-A) for constructability and reduction of sensor-to-sensor interaction.

Centrifuge facilities that could accommodate sensors in addition to the required sensors were encouraged to include the highly recommended and recommended sensors. The recommend sensors are at equivalent depths as sensors in the central array intended to help in understanding the effect of the container boundaries on the model response. Details of the centrifuge tests conducted by each experimental group are reported in separate papers published in this special edition of the Journal [15,25,32,37,52,66].

3. Soil characterization and element tests

The selected soil, Ottawa sand F-65, was characterized through a series of standard laboratory tests to determine its particle size distribution, specific gravity, and coefficient of hydraulic conductivity. The results of all these tests were made available to the predictors. These results are also documented in Vasko [54] and the data may be accessed via the LEAP database [13,14].

In addition to the above mentioned tests, a series of monotonic drained and undrained compression and extension tests were conducted on samples of Ottawa sand prepared by tapped-dry pluviation [29]. The monotonic tests were performed with three different initial void ratios and under a range of initial confining pressures. Fig. 3 shows the results of drained compression tests performed with an initial density of

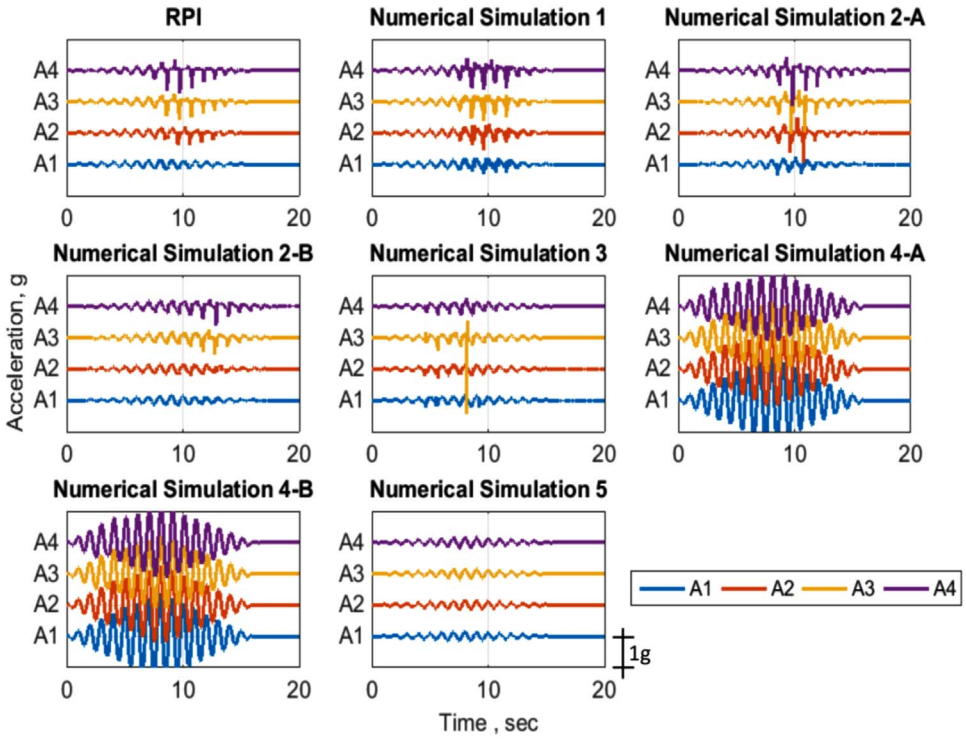

Fig. 8. Comparison of type A simulations of acceleration time histories at the location of A1 to A4 with the results of the reference experiment, Motion #2 (see Fig. 1 for transducer locations.).

RMSE

	A1	A2	A3	A4
NS 1	0.3443	0.3565	0.4058	0.4539
NS 2-A	0.3526	0.4668	0.5014	0.5436
NS 2-B	0.3429	0.3632	0.4336	0.4576
NS 3	0.3221	0.3374	0.6834	0.3929
NS 4-A	3.0433	2.6911	2.5247	2.4793
NS 4-B	3.0627	2.7461	2.5980	2.5607
NS 5	0.3392	0.3598	0.4005	0.4440

1652 kg/m^3 (the target density for the preparation of the centrifuge test specimen).

To characterize the liquefaction resistance of the soil, a number of cyclic strain-controlled and stress-controlled undrained tests were conducted. These tests were conducted for the relative density intended in the centrifuge tests. The results of all these tests can be found in Vasko [54] and the LEAP database [13,14]. Fig. 4 shows the liquefaction strength curve obtained from strain-controlled and stress-controlled cyclic undrained tests. In strain-controlled tests, liquefaction state is reached when excess pore water pressure ratio reaches 100%. In stress-controlled tests, a single amplitude strain of 2.5% is used as criteria for liquefaction triggering.

The results of the monotonic and cyclic strain-controlled tests were made available to the predictors in the type A simulation exercise (i.e., before the event prediction exercise). At the start of the type A simulation phase, stress-controlled cyclic triaxial tests had not been completed yet. However, the results of these tests became available in the type C simulations for Motion #2 and type B simulations for Motion #4. A summary of the timeline of the simulations and the data provided to predictors are shown in Table 3.

4. True prediction exercise: comparisons with the observed responses

The results of soil characterization tests and the element test data discussed in Section 3 were provided to the numerical predictors for calibration of the constitutive models and for preparation of blind “True Prediction” of the centrifuge test. Details of the

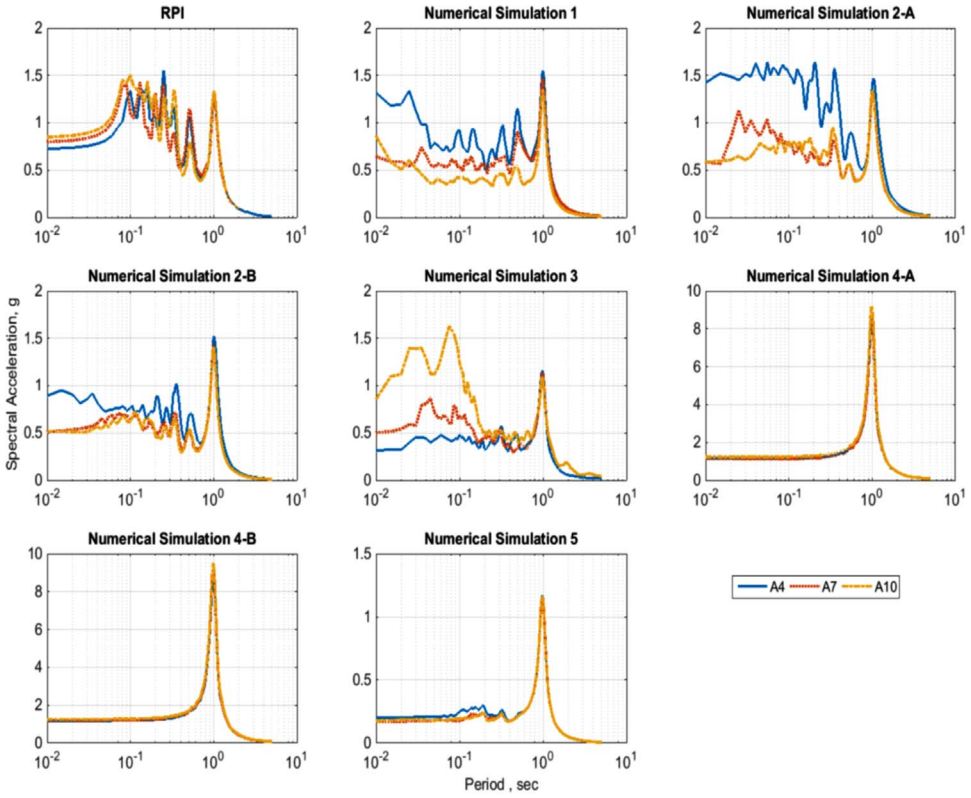

Fig. 9. Comparison of acceleration response spectra computed for type A simulations of the reference test along the same elevation near the soil surface, Motion #2 (see Fig. 1 for transducer locations.).

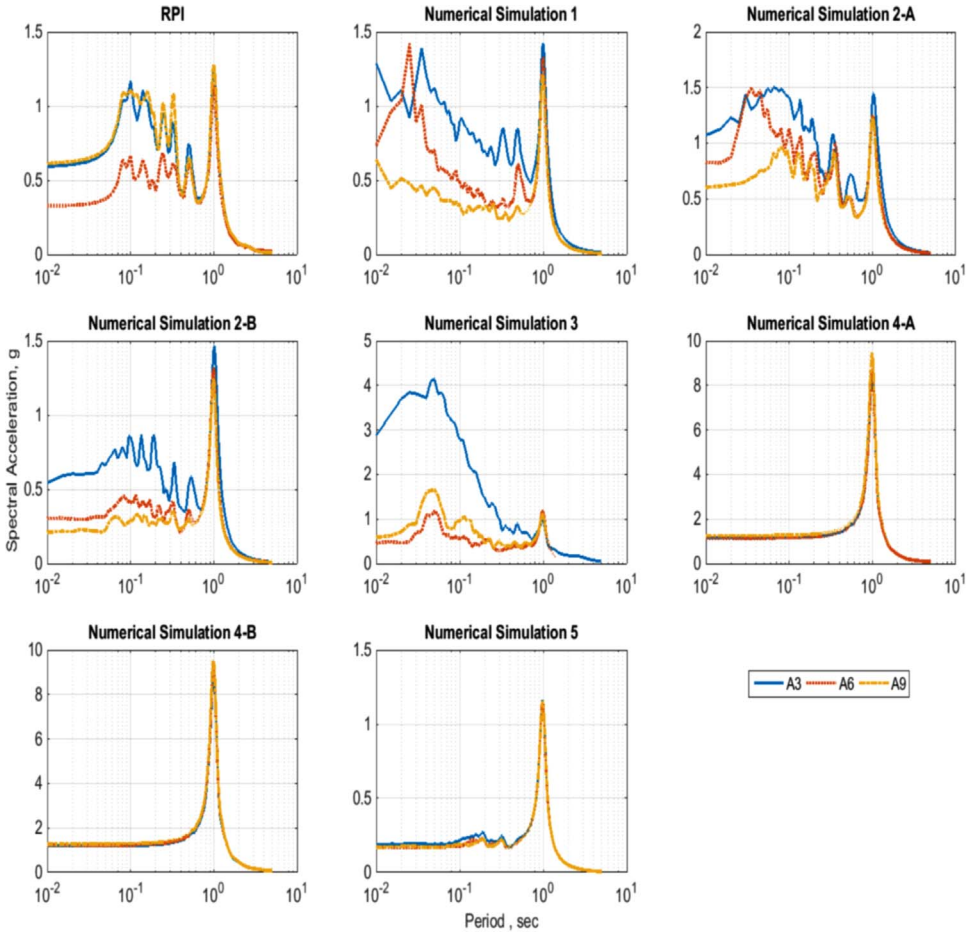

Fig. 10. Comparison of acceleration response spectra for type A simulations of the reference test along the same elevation, Motion #2 (see Fig. 1 for transducer locations.).

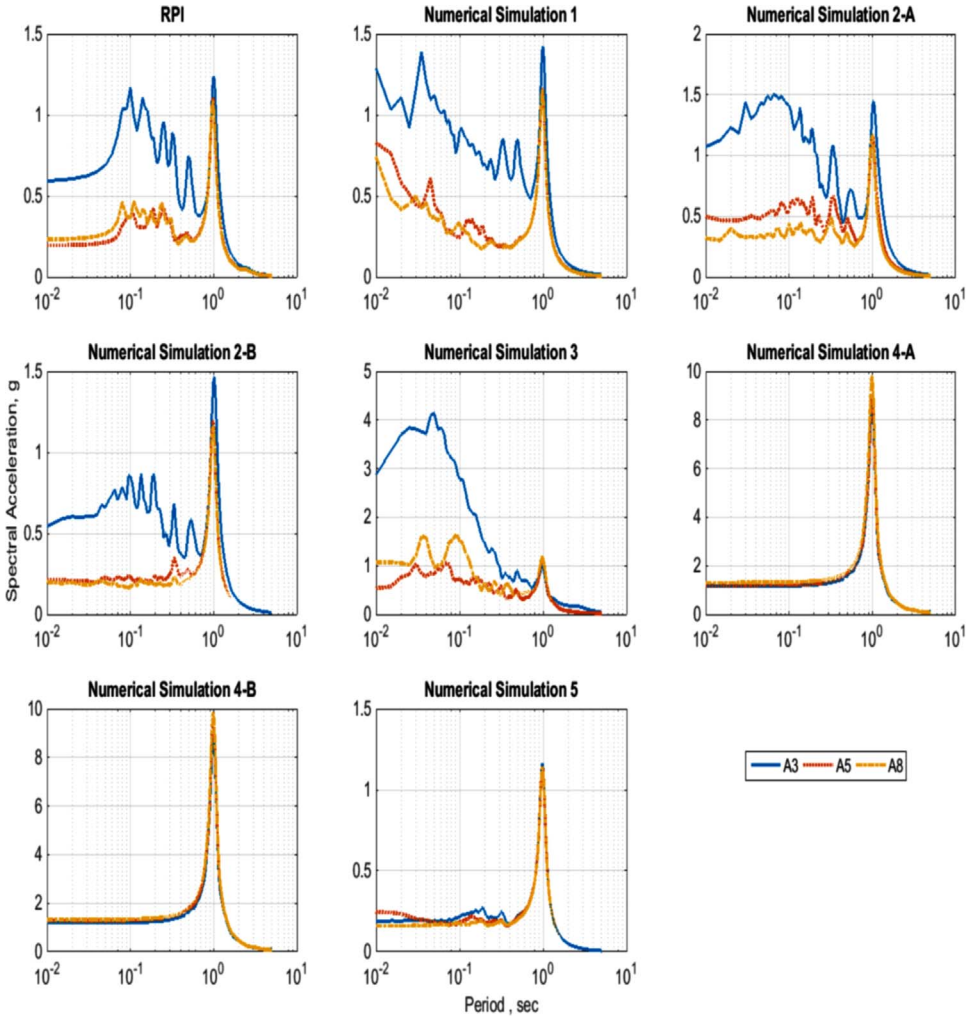

Fig. 11. Comparison of acceleration response spectra for type A simulations of the reference test along the same elevation, Motion #2 (see Fig. 1 for transducer locations.).

specifications for the centrifuge test including the soil density, sensor locations, geometry of the soil surface, and base excitation were also provided. The predictors submitted their predictions with a prescribed format. These predictions were reported in two phases. In the first phase, predictors were asked to submit their prediction of the response of the soil specimen shown in Fig. 1 to the prescribed base excitation with a maximum amplitude of 0.15*g*, known as Motion #2 [35]. These "*true predictions before the event*" are labeled here as type A simulations. After the submission of the type A simulations, the centrifuge tests were conducted and the results of the tests for Motion #2 were distributed to the predictors. They were then informed of nonconformities between the experiments and specifications for the experiments, including the measured base input motion, and asked to submit a type C simulation for Motion #2 using the measured input and important nonconformities. At this time, the predictors also submitted a type B simulation of the tests that followed Motion #2 using a larger base excitation with a maximum of 0.25*g* (known as Motion #4). It is important to note that at this stage, the actual recorded input Motion #4 was not yet distributed to the predictors, who performed their Type B predictions using the target Motion #4.

In this section a summary of the comparisons between these predictions and a selected reference experiment are presented. The density, achieved base input motion, degree of saturation, soil surface geometry, and sensor locations affect the results. Because of inherent differences and experimental uncertainties, the experimental facilities had different levels of success achieving and precisely following all of the specifications. Although it is theoretically not rigorous to pass judgment on the quality of simulations by comparing them to one specific experiment, to help in the visualization of the results, all simulations are presented

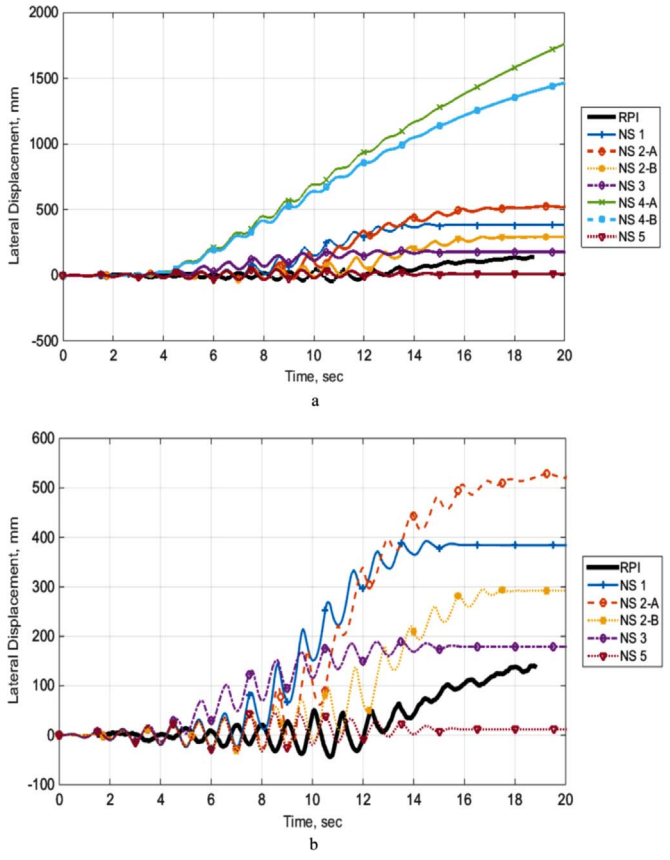

Fig. 12. a. Comparison of Type A simulations of lateral displacement time histories with the results of the RPI Test, Motion #2. b. Comparison of Type A simulations of lateral displacement time histories with the results of the RPI Test, Motion #2.

alongside a selected reference experiment. The RPI experiment was selected as a reference because it reproduced more accurately the specified input motion and included the measurements of lateral surface displacements. More rigorous evaluation of the numerical models should consider the comparisons with results from all of the centrifuge tests. Also, as shown in Kutter et al. [35], the lateral displacements of the RPI experiment were near the median of the displacements observed in other experiments so from this viewpoint the RPI experiment is also a good choice for the reference experiment. However, it should be noted that the pore water pressures recorded at RPI were slightly smaller than the median pore pressures, and the pore pressures in the RPI experiment dissipated faster than the pore pressures at most of the facilities.

Details of the constitutive models and numerical modeling techniques used by each predictor and all of the parameters used in the simulations are reported in separate papers published in this special edition of the Journal [24,3,5,53,68].

Figs. 5–7 show comparisons of the excess pore water pressures numerical simulations with the selected reference centrifuge test results. The simulations are numbered from 1 to 5. In cases where a predictor submitted two predictions, they are labeled A and B. The table at the bottom of each figure shows the root mean square of the difference between the prediction and experiment for the first 16 s of the record (RMSE-t16) which spans the duration of the base excitation and RMSE-t30 averages over the first 30 s of the record and spans some of the dissipation time. The 30-s period was used because predictors were asked to report the first 30 s of the simulations. The RMSE is calculated as:

$$RMSE = \sqrt{\frac{1}{N}\sum_{N}(R_u^e - R_u^s)^2} \tag{1}$$

N is the number of increments for the calculation period (16 or 30 s), R_u^e and R_u^s are the excess pore pressure ratios obtained at the same time from the experiment and simulation, respectively.

Fig. 5 shows that majority of the numerical simulations of excess pore pressure time histories in the central array (P1 to P4) were able to capture the maximum excess pore water pressures generated in these locations. Simulations 3 and 5 predicted significantly smaller excess pore water pressure. The reasons of these discrepancies are discussed in the separate papers by predictors published in this special edition of the Journal [24,3,5,53,68]. Furthermore, the numerical simulations (NS) show either a faster pace of dissipation (NS 1) or a much slower dissipation (NS 2A, NS 4A, NS 4B). Prediction of excess pore pressure time histories near the vertical boundaries of the box (i.e. left and right arrays of sensors) appear to be more challenging. Nevertheless, the trends produced in several predictions (e.g., NS 1, NS 2B, NS 3) are consistent with the observed responses.

Fig. 6 shows detailed comparisons of the predicted excess pore water pressure time histories with the measured responses in the left array of sensors at the top of the slope (P5 and P6). The predicted trends show a net positive excess pore pressure at location of P5 with significant oscillations. This trend is consistent with the measured response of the excess pore pressure at P5. However, the predicted dissipation rates of the excess pore pressure were faster than the experimentally observed trend in some simulations (1) and slower in some other cases (NS 2-A, NS 4-A). As expected the measured excess pore pressure at P6 showed relatively large negative spikes of pore water pressure, which are evidence of dilatancy. This trend was reasonably simulated in numerical simulations NS 1, NS 2-A, NS 2-B, and NS 3. Numerical simulations NS 4-A and NS 4-B showed positive excess pore pressure during the shaking phase and significant negative excess pore pressure after the end of the shaking.

Fig. 7 shows detailed comparisons of the predicted excess pore water pressure time histories with the measured responses in the right array of sensors at the bottom of the slope (P7 and P8). Compared to the pore pressure time histories measured at the top of the slope (P5, P6), less dilative responses were observed in the pore water pressure time histories measured at locations of P7 and P8. Except for NS 3 and NS 5, the simulated responses also show a less dilative trend during the shaking phase.

Fig. 8 shows similar comparisons for the acceleration time histories (A1 to A4). The RMSE values for accelerations are computed using the acceleration response spectra, i.e.:

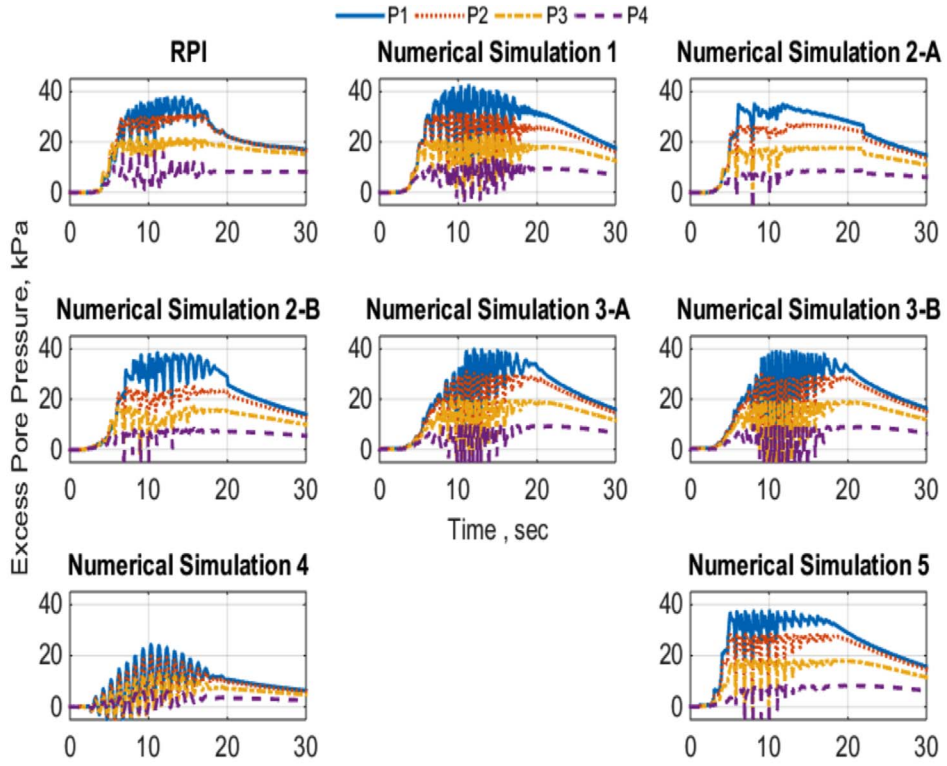

Fig. 13. Comparison of type B simulations of excess pore water pressure time histories computed at the location of P1, P2, P3, and P4 with the results of the RPI Test, Motion #4 (see Fig. 1 for transducer locations.).

RMSE-t16

	P1	P2	P3	P4
NS 1	0.1419	0.2231	0.3007	0.4834
NS 2-A	0.1188	0.1234	0.1837	0.2835
NS 2-B	0.0942	0.2130	0.3025	0.3304
NS 3-A	0.1500	0.2598	0.3801	0.5476
NS 3-B	0.1873	0.3060	0.4725	0.8398
NS 4	0.3886	0.5191	0.5879	0.6118
NS 5	0.2008	0.1965	0.2075	0.3391

RMSE-t30

	P1	P2	P3	P4
NS 1	0.1503	0.1813	0.2280	0.3638
NS 2-A	0.1037	0.1026	0.1593	0.2227
NS 2-B	0.0885	0.1709	0.2588	0.2660
NS 3-A	0.1484	0.2049	0.2853	0.4047
NS 3-B	0.1657	0.2361	0.3512	0.6176
NS 4	0.3509	0.4719	0.5637	0.5635
NS 5	0.1624	0.1535	0.1633	0.2548

$$RMSE = \sqrt{\frac{1}{N}\sum_{N}(S_a^e - S_a^s)^2} \tag{2}$$

Damping ratio of 5% and a total period of 5 s was considered in the calculation of EMSE values for accelerations. Except for predictions 4A and 4B, the predicted acceleration time histories in the central array (A1 to A4) are reasonably close to the observed responses at these locations.

Figs. 9–11 show a comparison of the acceleration response spectra for the type A simulations of the reference test. Fig. 9 shows a comparison of the accelerations at locations A4, A7, and A10. It is interesting to note that for these locations that are in a plane parallel to the specimen free surface, accelerations recorded in the left and right array (A7 and A10) are quite close. The effect of boundary on the measured responses is less pronounced. However, majority of simulation show larger differences between the accelerations computed at A7 and A10. Figs. 10 and 11 show similar comparisons for the accelerations are also parallel to the specimen free surface but are computed at deeper locations that A7 and A10. Here more pronounced effects of right and left boundaries are observed.

Fig. 12a shows a comparison of the predicted lateral displacements for a point in the mid length and top surface of the soil specimen. The lateral displacement time history in the reference experiment is the average displacement of the markers placed at the center of the soil surface obtained from the processing of the images taken by a high speed camera. Here again, except for predictions NS 4A, NS 4B, and NS

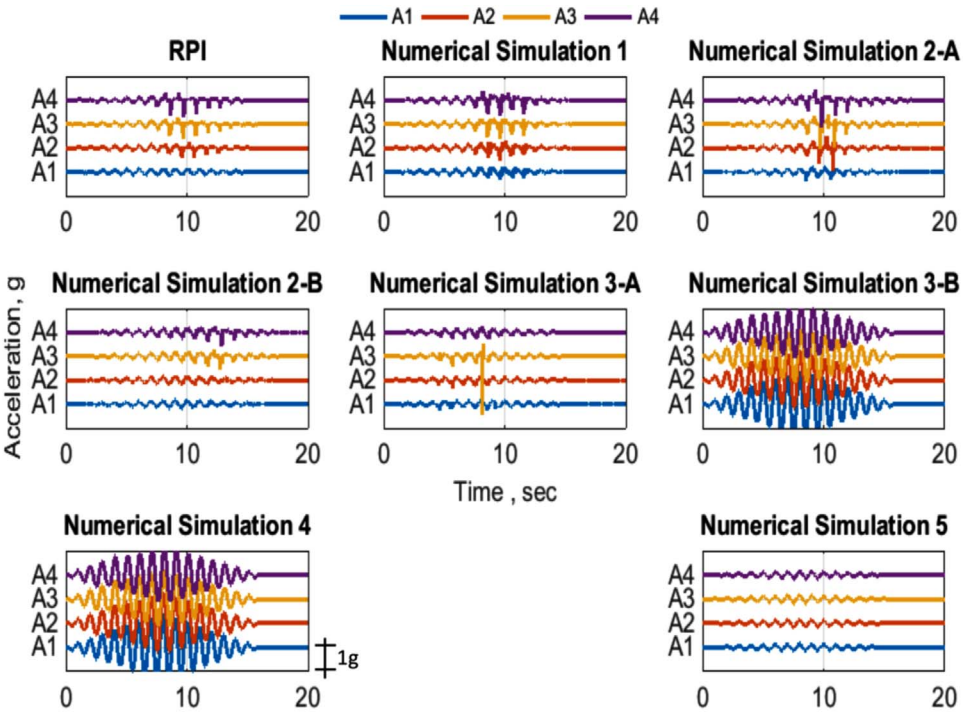

Fig. 14. Comparison of type B simulations of acceleration time histories computed at the location of A1 to A4 with the results of the RPI Test, Motion #4 (see Fig. 1 for transducer locations.).

RMSE

	A1	A2	A3	A4
NS 1	0.1131	0.2059	0.2911	0.3313
NS 2-A	0.0609	0.1740	0.2026	0.2232
NS 2-B	0.1252	0.1304	0.1343	0.1892
NS 3-A	0.0392	0.1796	0.1553	0.1517
NS 3-B	0.0261	0.0809	0.1518	0.1721
NS 4	0.0612	0.2468	0.2775	0.3702
NS 5	0.1233	0.1504	0.1685	0.2303

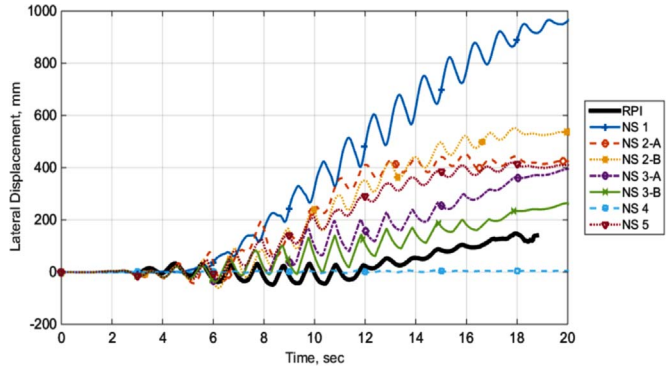

Fig. 15. Comparison of the type B simulation of lateral displacement time histories for Motion #4 with the results of the RPI Test, Motion #4 (see Fig. 1 for transducer locations.).

Table 2
Participants in the prediction exercise (listed alphabetically).

Participant name	Constitutive model	Analysis platform
Richard Armstrong	PM4Sand (v 3)	FLAC 7
Michael Beaty	UBC Sand (v 904aR)	FLAC 7
Alborz Ghofrani – Pedro Arduino	Dafalias and Manzari [17]	OpenSEES
Nithyagopal Goswami	PDMY	OpenSEES
Kyohei Ueda	Cocktail Glass Model	FLIP-TULIP
Katerina Ziotoupoulou	PM4Sand (v 3)	FLAC 7 [30]

5, the predicted lateral displacement time histories shows similar trends to the observed displacement time history. Since NS 4A and NS 4B significantly over-predict the lateral displacement, to allow for a better comparison of the predicted displacements with the measured displacement time history, the same comparisons but without the simulations NS 4A and 4B are shown in Fig. 12b.

5. Types B and C simulations

Following the submission of the type A simulations for Motion #2 (with a maximum acceleration of 0.15*g*), the results of the centrifuge experiments conducted at different facilities were made available to all the predictors and they were asked to submit a type B simulation for

Table 3
Timeline of the LEAP-GWU prediction exercise.

12/15/2014	• Predictors were provided with: the test configuration, the results of monotonic triaxial tests, strain-controlled cyclic traixial tests, and standard tests (sieve analysis, specific gravity, and permeability tests)
01/15/2015	• Due date for submission of true predictions. • Majority of centrifuge tests were completed.
01/26-27/2015	• LEAP-GWU workshop was held: The results of centrifuge tests for motion #2 and a summary of comparisons between the true predictions and the selected reference centrifuge test were presented
04/06/2016	• Predictors were provided with the results of the centrifuge tests on all sites for Motion #2, the achieved base motion for Motion #4, and the results of stress-controlled cyclic triaxial tests. They were asked to submit type B Simulations for Motion #4 and type C simulations for Motion #2
06/15/2015	• Due date for submission of the type B and type C simulations

Motion #4 (with a maximum acceleration of 0.25*g*). Achieved base excitations for Motion #4 were also made available to the predictors. In this round of simulations, predictor 3 submitted two sets of simulations that are labeled NS 3A and NS 3B.

Figs. 13–15 show comparisons among the numerical simulations and with the recorded data at RPI. In these comparisons, the focus is only on the responses along the central array of sensors. Detailed comparisons of the simulated responses with the observations at other available sensors (left and right arrays) are presented in an Electronic supplement to this paper.

The excess pore pressure comparisons (Fig. 13) show significant improvements in some of the predictions compared to those observed in the type A simulations. In particular, the majority of excess pore water pressure time histories (except for numerical simulation 4) show trends consistent with the observed responses. The significant improvements in the rate of dissipation of excess pore water pressures are particularly striking.

Majority of the presented acceleration time histories also show reasonably good agreement with the observed responses (Fig. 14).

The simulated lateral displacement time histories show similar trends but larger values than that observed in the RPI experiment (Fig. 15). Simulation NS 1 shows a large over-prediction, while simulation NS 4 significantly under-predicts the lateral displacements observed in the free surface of the soil specimen.

Following the submission of the type B simulations, the results of all the centrifuge tests obtained in the five centrifuge facilities were provided to the predictors and they were asked to submit an after the event assessment (type C simulation) of the test results for motions #2. As shown in Table 3, in addition to the results of centrifuge tests for Motion #2, the predictors were provided with the results of a series of cyclic stress-controlled tests (Fig. 4) to allow for possible re-calibration of the constitutive models, if necessary (Tables 2 and 3).

Figs. 16–18 show comparisons of the numerical simulations with the recorded data at RPI. In these comparisons, the focus is only on the responses observed in the central array of sensors. Detailed comparisons of the simulated responses with the observations at other available sensors (left and right arrays) are presented in an Electronic supplement to this paper.

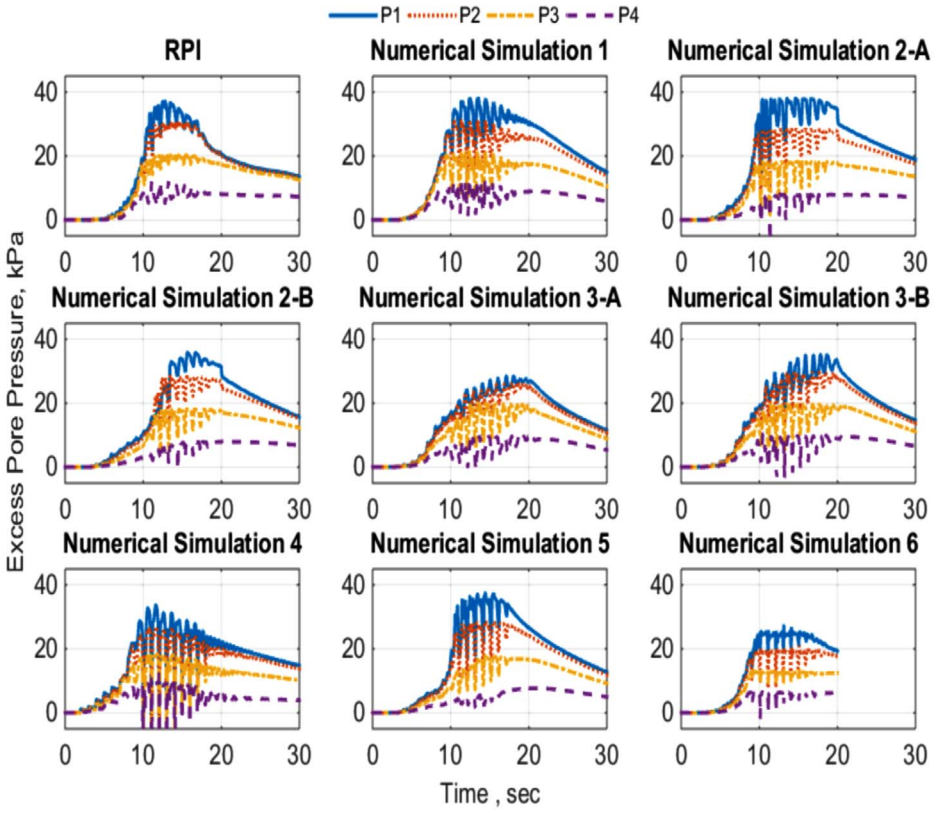

Fig. 16. Comparison of type C simulations of excess pore water pressure time histories computed at the Location of P1, P2, P3, and P4 with the results of the RPI Test, Motion #2 (see Fig. 1 for transducer locations.).

RMSE-t16

	P1	P2	P3	P4
NS 1	0.1059	0.1746	0.1968	0.2838
NS 2-A	0.0959	0.1379	0.1578	0.1989
NS 2-B	0.1637	0.1629	0.1913	0.2502
NS 3-A	0.1722	0.1787	0.1792	0.2696
NS 3-B	0.1201	0.1364	0.1604	0.2720
NS 4	0.2118	0.2742	0.3037	0.4099
NS 5	0.0781	0.1249	0.1983	0.2859
NS 6	0.1436	0.2234	0.2126	0.1950

RMSE-t30

	P1	P2	P3	P4
NS 1	0.1416	0.1625	0.1514	0.2187
NS 2-A	0.1648	0.1568	0.1270	0.1522
NS 2-B	0.1611	0.1510	0.1472	0.1897
NS 3-A	0.1402	0.1479	0.1513	0.2134
NS 3-B	0.1416	0.1460	0.1318	0.2178
NS 4	0.1626	0.2135	0.2609	0.3758
NS 5	0.0919	0.1095	0.1608	0.2278
NS 6	N/A	N/A	N/A	N/A

In addition to the simulations by the predictors who participated in the type A simulation exercises, one additional set of simulations are included in these Figures. This additional set of simulations (NS 6) was submitted by Nithyagopal Goswami of RPI who used the UCSD sand model implemented in OpenSees.

On Fig. 16 the root mean square error (difference between the simulation and the measured value) were calculated for each simulation. Since the base excitation is only 16 s, the RMSE values were calculated for both the first 16 s and the entire period of 30 s for which both simulations and experimental results were available.

The comparisons presented in Fig. 16 show significant improvements in simulation of excess pore pressure time histories in the central array (P1 to P4) over the simulations submitted in the true prediction phase refer to the corresponding figure). The maximum excess pore pressures simulated in majority of numerical simulations (except in simulations NS 3-A and NS 6) were reasonably close to the measured responses. However majority of simulated excess pore pressures showed significant oscillations, indicating large dilative response, once

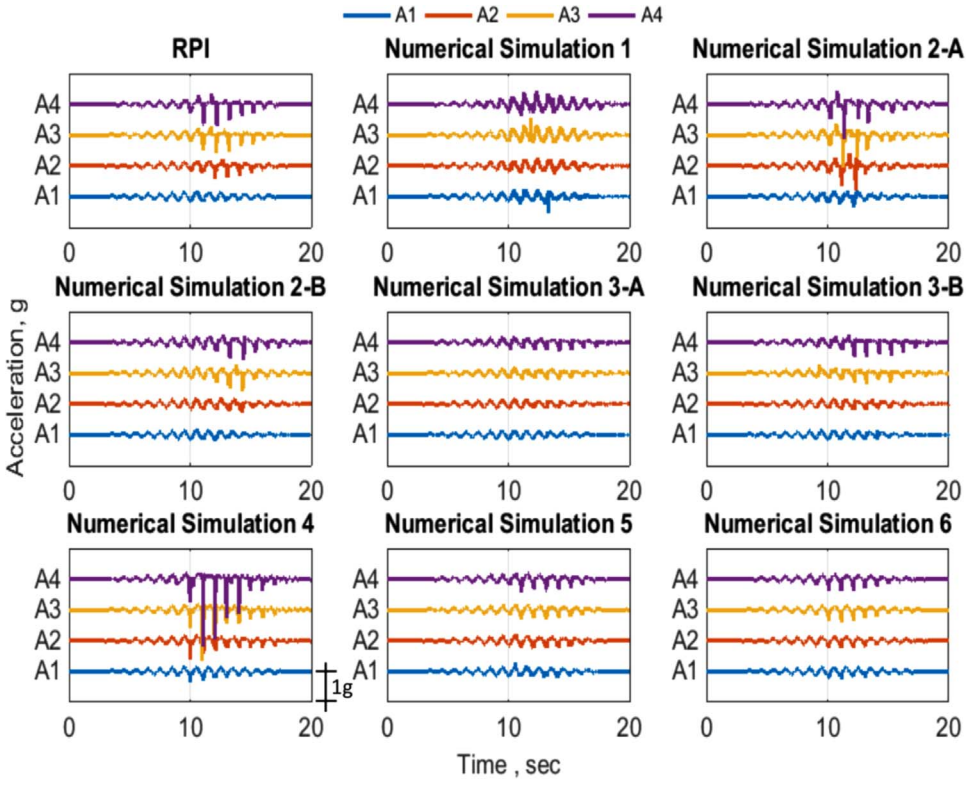

Fig. 17. Comparison of type C simulations of acceleration time histories computed at the Location of A1 to A4 with the results of the RPI Test, Motion #2 (see Fig. 1 for transducer locations.).

RMSE

	A1	A2	A3	A4
NS 1	0.0510	0.1075	0.1547	0.2009
NS 2-A	0.0646	0.1316	0.1438	0.1568
NS 2-B	0.0156	0.0709	0.0769	0.1227
NS 3-A	0.0229	0.1036	0.1720	0.2193
NS 3-B	0.0250	0.0907	0.1402	0.1473
NS 4	0.0320	0.0754	0.2022	0.3238
NS 5	0.0279	0.0791	0.1334	0.1884
NS 6	0.0208	0.0822	0.1227	0.1899

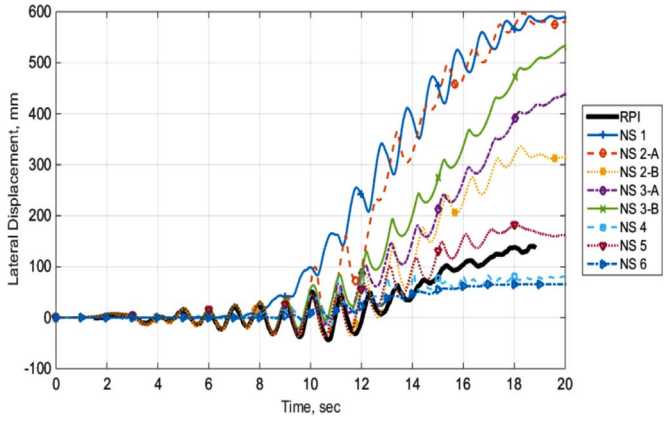

Fig. 18. Comparison of type C simulations of lateral displacement time histories with the results of the RPI Test, Motion #2 (see Fig. 1 for transducer locations.).

maximum excess pore pressure was reached. The simulated dissipation rates were also improved in majority of the simulations.

Fig. 17 show a comparison of acceleration time histories with the measured responses in the RPI test. Numerical simulations NS 4 showed close correspondence with the experimental results at locations of A1 and A2, but produced relatively large spikes in acceleration time history A4. The numerical simulations NS 2-B and NS 3-B presented the least RMSE values for most acceleration time histories.

The simulated time histories of lateral displacement on the specimen surface in Fig. 18 showed less scatter compared to the predictions submitted in the true prediction phase (Fig. 12). Compared to all the presented simulations, the simulations NS 4, NS 5, and NS 6 were closer to the measured response by a factor of about 2. Majority of the simulations were able to capture the dynamic component of lateral displacement (cyclic oscillations) reasonably well.

Figs. 19–32 show the comparison of the type C simulations with the centrifuge test results for Motion #2 obtained at UC Davis, Kyoto University, National Central University of Taiwan (NCU), Cambridge University, and Zhejiang University (ZU), respectively.

Fig. 19 shows that numerical simulations NS 1, NS 2-A and NS 3-B closely simulated the excess pore pressure generation during shaking measured in the central array of the UCD experiment. As this was a type C simulation, the predictors were informed of the nonconformity between specified and actual viscosity used in the UCD experiment, but apparently this message was not clear to the predictors as they did not

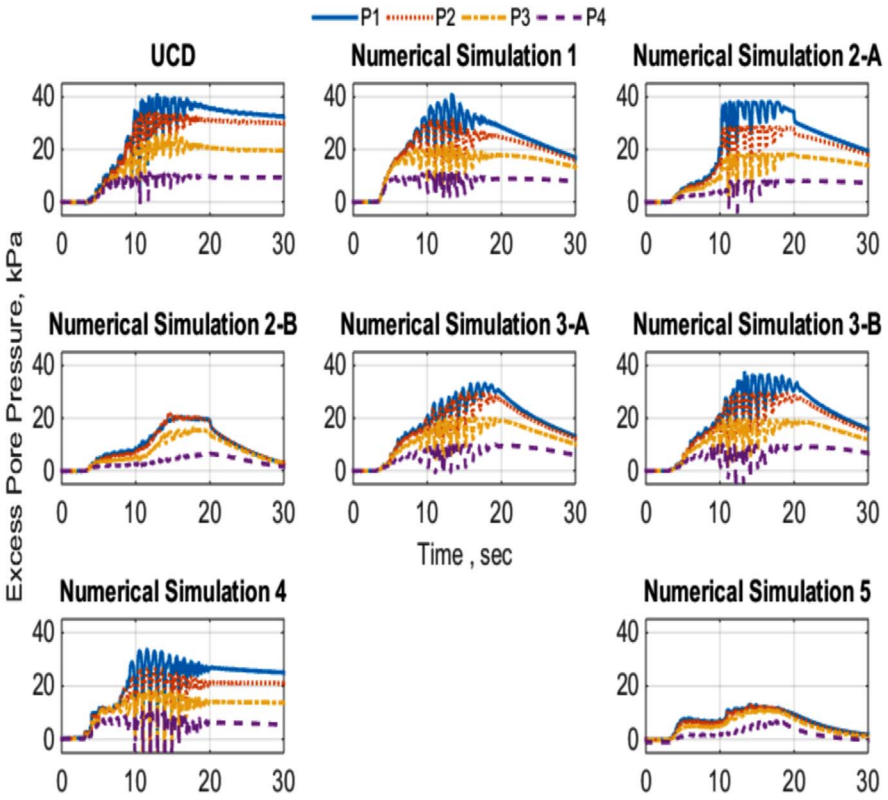

Fig. 19. Comparison of type C simulations of excess pore water pressure time histories computed at the Location of P1, P2, P3, and P4 with the results of the UCD Test, Motion #2 (see Fig. 1 for transducer locations.).

RMSE-t16

	P1	P2	P3	P4
NS 1	0.1862	0.2216	0.2948	0.3199
NS 2-A	0.1654	0.1973	0.2507	0.3569
NS 2-B	0.3301	0.3580	0.3902	0.4641
NS 3-A	0.1766	0.1881	0.2305	0.3149
NS 3-B	0.1629	0.1711	0.2475	0.3348
NS 4	0.2349	0.2915	0.3524	0.4405
NS 5	0.3859	0.4251	0.4045	0.4684

RMSE-t30

	P1	P2	P3	P4
NS 1	0.2215	0.2635	0.2566	0.2456
NS 2-A	0.1818	0.2241	0.2329	0.2912
NS 2-B	0.4617	0.5154	0.4770	0.4866
NS 3-A	0.2472	0.2780	0.2476	0.2540
NS 3-B	0.2068	0.2341	0.2396	0.2722
NS 4	0.2256	0.3050	0.3402	0.4000
NS 5	0.5529	0.6351	0.5954	0.6020

account for the reduced permeability in the type C simulations of the UCD experiment, hence the predictions did not simulate the slower rate of dissipation observed.

Fig. 20 shows that the simulated acceleration time histories at UCD in general had larger RMSE values as compared to the type C simulations submitted for the RPI test. Similar pattern is observed in simulation of lateral displacements shown in Fig. 21. Except for numerical simulation NS 4, the magnitudes and in some cases (NS 2-A and NS 2-B) the trends of the simulated displacement time histories were quite different from the response observed in the experiment. It should be noted that in Fig. 21 the dynamic component of the displacement time history measured at UCD was computed from double integration of the measured acceleration time history in Fig. 20, measured near the specimen surface, and combined with the final permanent displacement measured at the end of the test using surface markers. This final permanent displacement was superimposed on the dynamic displacement time history to construct the hybrid computed-measured time for lateral displacement on the free surface of the soil specimen plotted in Fig. 21 for UCD. A similar technique was also used to construct the time histories of lateral displacement for KU, CU and ZJU (Figs. 24, 30, and 33). No permanent displacements were available for the NCU test. Hence the measured lateral displacement time history for NCU in Fig. 27 only shows the dynamic component computed from the double-integrated acceleration time history. In all cases, the computed dynamic component of the displacement, integrated from the acceleration data, is considered to be highly reliable. But although the magnitude of the permanent lateral displacement is also accurate, the timing of the maximum displacement is based on a viable interpolation function, not

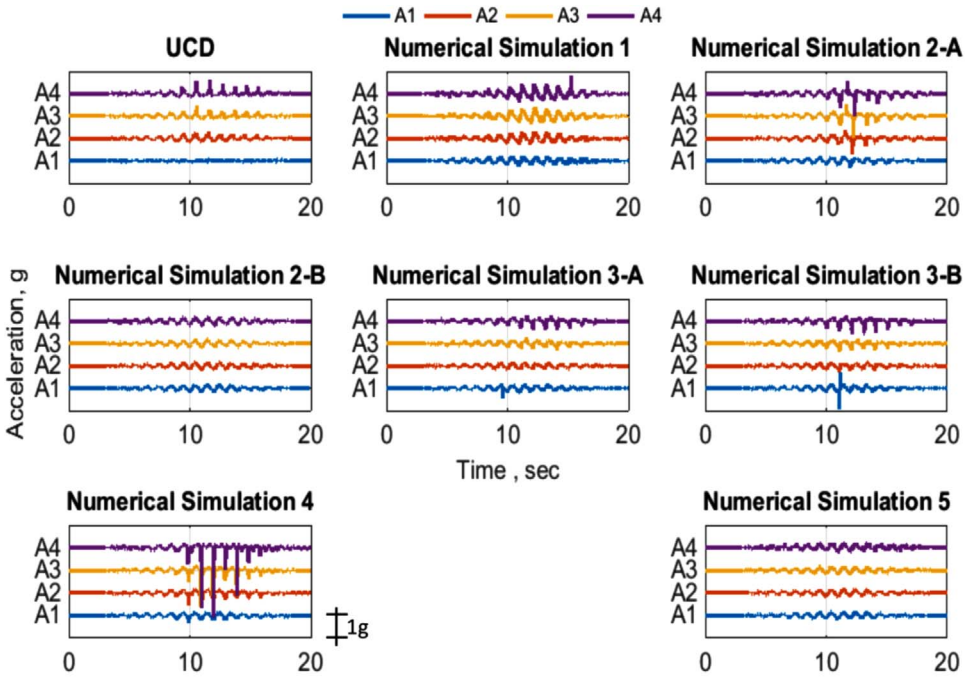

Fig. 20. Comparison of type C simulations of acceleration time histories computed at the location of A1 to A4 with the results of the UCD Test, Motion #2 (see Fig. 1 for transducer locations.).

RMSE

	A1	A2	A3	A4
NS 1	0.1999	0.1182	0.1736	0.2069
NS 2-A	0.2025	0.1661	0.1946	0.1572
NS 2-B	0.1789	0.0204	0.0980	0.1728
NS 3-A	0.1710	0.0426	0.0735	0.1176
NS 3-B	0.2073	0.0418	0.0527	0.0690
NS 4	0.1839	0.0814	0.2183	0.4385
NS 5	0.1738	0.0297	0.1060	0.1759

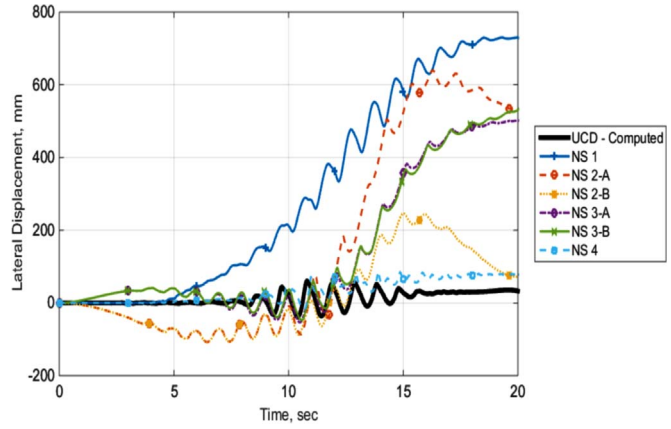

Fig. 21. Comparison of the type C simulations of lateral displacement time histories with the results of the UCD Test, Motion #2 (see Fig. 1 for transducer locations.).

on measurements (as explained by [35] in this special issue of the Journal).

The simulations NS 1 and NS 2-A presented in Fig. 22 show reasonably good correlations with the excess pore pressure time histories measured in the central array of the KU test. Simulations NS 2-B and NS 5 showed much less excess pore pressure generation when compared to the measured pore pressures.

Fig. 23 shows that except for some large spikes in simulation NS 3-A (A3) and NS 4 (A4), the acceleration time histories simulated for the KU test showed good agreement with the measured responses.

Fig. 24 shows that simulation NS 2-B, NS 4, and NS 6 led to final displacements that are reasonably close to the measured lateral displacement in the KU test. Fig. 24 shows that the simulations NS 1, NS 2-A, NS 3-B have led to significantly larger displacements while simulation NS 5 led to significantly smaller displacement.

Fig. 25 shows the simulated excess pore pressures for the NCU test. Here the measured excess pore pressure at location of P3 contained significant noise. The excess pore pressure measured at P1 was generally higher than those simulated by predictors. However several

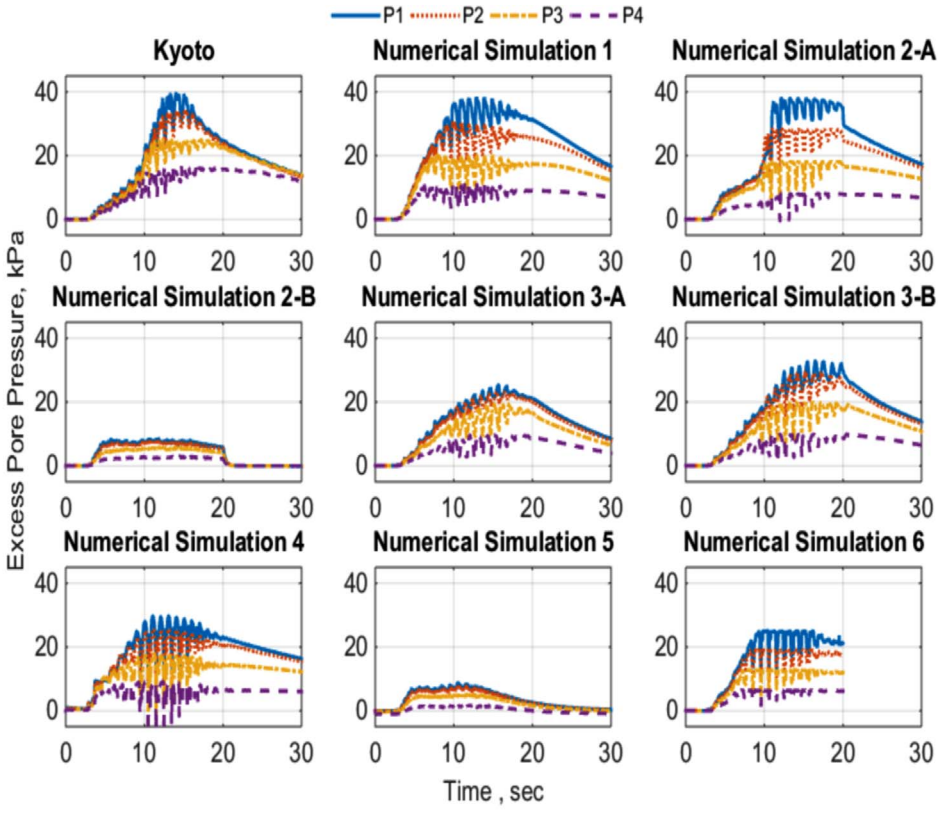

Fig. 22. Comparison of type C simulations of excess pore water pressure time histories computed at the Location of P1 to P4 with the Results of the Kyoto University (KU) Test, Motion #2 (see Fig. 1 for transducer locations.).

RMSE-t16

	P1	P2	P3	P4
NS 1	0.2061	0.2670	0.3060	0.3904
NS 2-A	0.0914	0.1369	0.2334	0.4611
NS 2-B	0.3818	0.4465	0.5190	0.7029
NS 3-A	0.1895	0.2035	0.2465	0.4269
NS 3-B	0.1244	0.1332	0.2022	0.3831
NS 4	0.1902	0.2467	0.3161	0.4939
NS 5	0.3945	0.4646	0.5517	0.7979
NS 6	0.1901	0.2559	0.3214	0.4750

RMSE-t30

	P1	P2	P3	P4
NS 1	0.1735	0.2069	0.2653	0.5118
NS 2-A	0.1149	0.1207	0.2337	0.5905
NS 2-B	0.4360	0.5406	0.7263	1.0739
NS 3-A	0.1648	0.1900	0.2992	0.5971
NS 3-B	0.1003	0.1063	0.2024	0.4967
NS 4	0.1475	0.1990	0.3182	0.6728
NS 5	0.4461	0.5541	0.7495	1.1669
NS 6	N/A	N/A	N/A	N/A

simulations were able to simulate the maximum magnitude of excess pore pressure at P2, P3, and P4 quite well.

Acceleration time histories recorded in the central array of the NCU test showed relatively large spikes at A2, A3, and A4 (Fig. 26). This trend is well captured in simulations NS 2-A and NS 4.

Fig. 27 shows a comparison of the lateral displacements simulated for the NCU test. In this case, since the final value of lateral displacement on the free surface is not measured, direct comparison with the simulation results is not possible. However the dynamic component of the computed displacement (Fig. 27) is reasonably simulated by many of the simulations.

Fig. 28 shows a comparison of the excess pore pressure time histories measured at CU with the simulated time histories in the central array. The maximum excess pore pressures measured at P2 and P4 appear to be smaller than expected values at these locations. Majority of the simulations showed larger excess pore pressures at these locations. It is noted that the achieved dry density in the CU test was 4.3% lower than the target density of 1652 kg/m^3 which leads to a relative density of 26–48% depending on the values of e_{max} and e_{min} reported by various investigators for Ottawa sand [15]. In principle, the predictors should consider this significant variation in the soil density in performing the AEA numerical simulations. However the discrepancy between densities was not accounted for by majority of the predictors.

Acceleration time histories recorded in the central array of the CU test did not show the large spikes observed in other experiments (Fig. 29), however several simulated acceleration time histories contained large spikes, particularly at the location of A4. This discrepancy

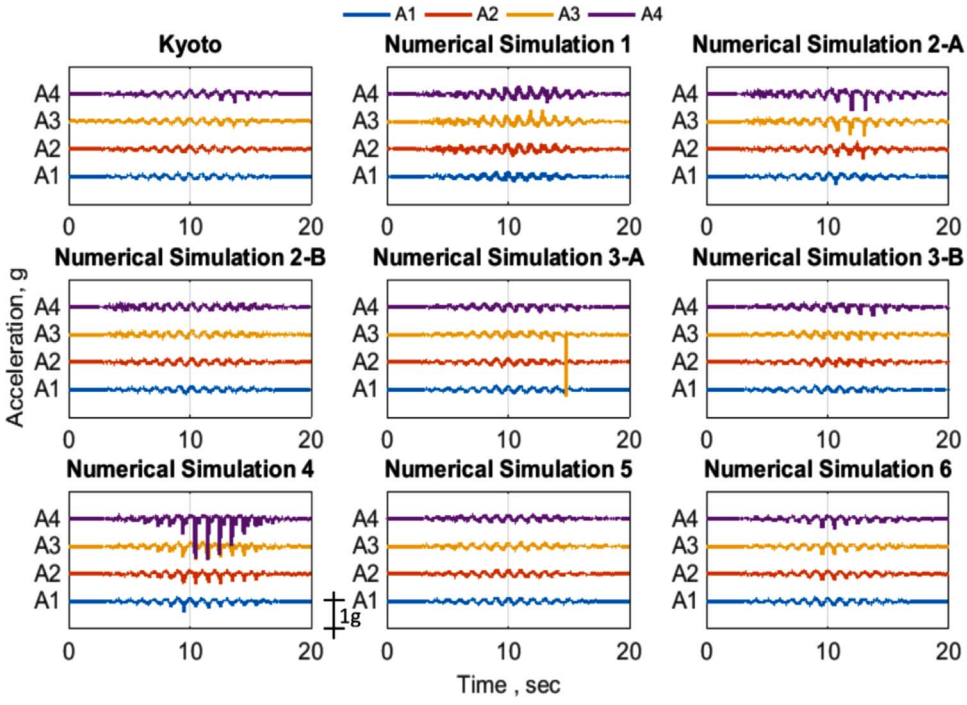

	A1	A2	A3	A4
NS 1	0.0477	0.0899	0.1222	0.1336
NS 2-A	0.0453	0.0959	0.1618	0.1684
NS 2-B	0.0201	0.0294	0.0450	0.0711
NS 3-A	0.0112	0.0100	0.1973	0.0566
NS 3-B	0.0104	0.0199	0.0251	0.0379
NS 4	0.0476	0.0693	0.1114	0.2651
NS 5	0.0114	0.0085	0.0286	0.0656
NS 6	0.0180	0.0389	0.0482	0.0353

Fig. 23. Comparison of type C simulations of acceleration time histories computed at the location of A1 to A4 with the Results of the Kyoto University (KU) Test, Motion #2 (see Fig. 1 for transducer locations.).

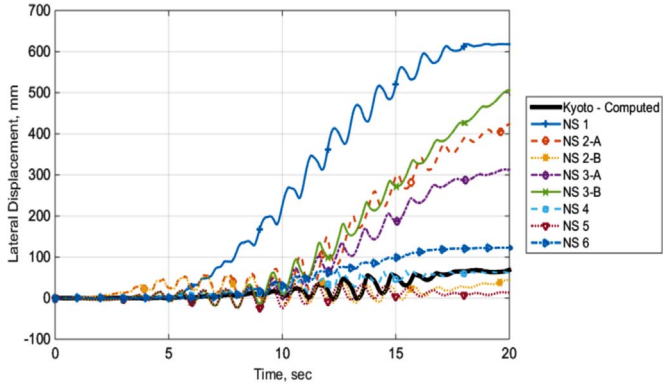

Fig. 24. Comparison of the type C simulations of lateral displacement time histories with the results of the Kyoto University (KU) Test, Motion #2 (see Fig. 1 for transducer locations.).

appears to be consistent with the looser packing of the soil in the CU test which was not considered in the simulations.

Fig. 30 shows a comparison of the lateral displacements simulated for the CU test. Except for Simulation NS 4, other simulations have predicted a larger lateral displacement that observed in the experiment.

Fig. 31 show a comparison of the type C simulations of excess pore pressure time histories with the results of the ZU Test. It is noted that predictor #2 did not submit an AEA simulation of the ZU test. Simulations NS 1, NS 3-B and NS 5 appear to have captured the trends observed at P1 and P2 reasonably well. The pore pressures measured at P2 and P3 showed larger oscillations about their maximum values as compared to those in the numerical simulations.

Fig. 32 shows a comparison of the simulated acceleration time histories for the ZU test with the measured values in the central array of sensors. Relatively large spikes are present in the measured time histories at A1, A2, and A4. This feature, albeit sometimes stronger, is replicated in the simulations.

The measured lateral displacement in the ZU test is much larger than the lateral displacements reported by other centrifuge facilities (Fig. 33). Simulations NS 1, NS 3-A and NS 3-B also show comparable magnitude for the final lateral displacements.

A summary of the RMSE values computed for types A, B, and C simulations of the RPI test are shown in Figs. 34 and 35 for the pore pressure and acceleration time histories, respectively. It is clearly observed that almost all the AEA simulations (after the event) show a reduced RMSE over the corresponding predictions made by the same

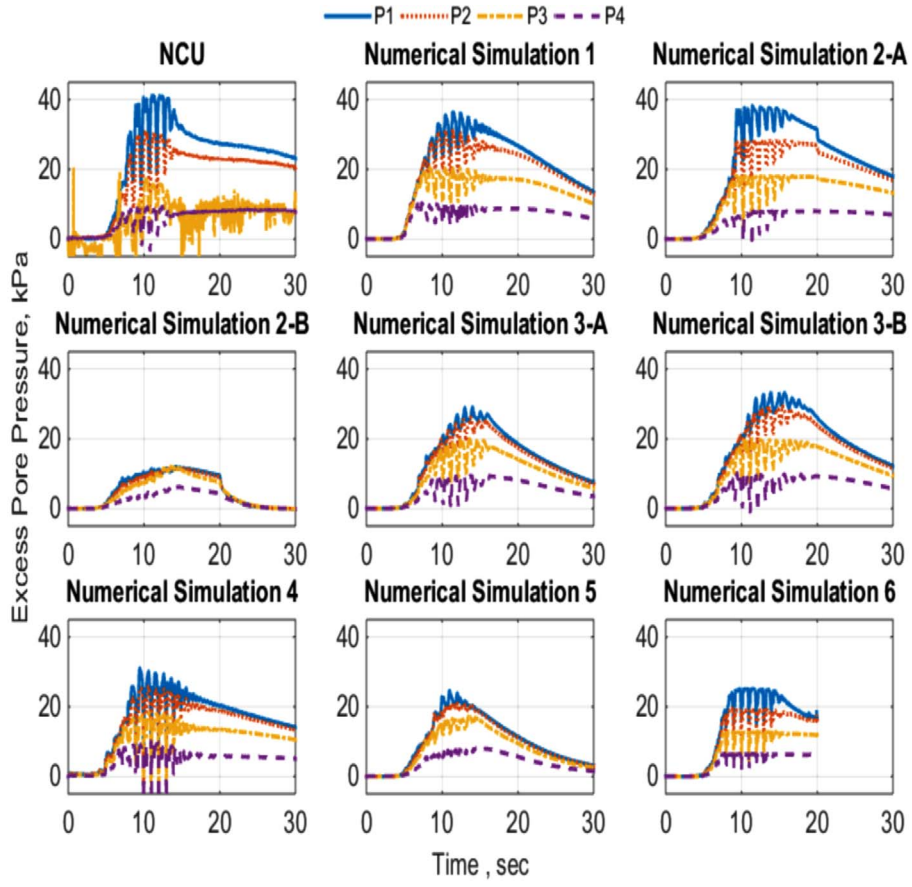

Fig. 25. Comparison of type C simulations of excess pore water pressure time histories computed at the Location of P1 to P4 with the Results of the NCU Test, Motion #2 (see Fig. 1 for transducer locations.).

RMSE-t16

	P1	P2	P3	P4
NS 1	0.1443	0.1946	0.4513	0.2934
NS 2-A	0.1568	0.1745	0.3583	0.2508
NS 2-B	0.4204	0.3484	0.2164	0.2511
NS 3-A	0.2262	0.1738	0.3400	0.2876
NS 3-B	0.2016	0.1719	0.3501	0.3028
NS 4	0.2343	0.2119	0.3695	0.3278
NS 5	0.2696	0.1881	0.3023	0.2145
NS 6	0.2256	0.2055	0.2703	0.2082

RMSE-t30

	P1	P2	P3	P4
NS 1	0.1393	0.1669	0.4189	0.2252
NS 2-A	0.1323	0.1413	0.3862	0.1879
NS 2-B	0.4924	0.4977	0.2709	0.4692
NS 3-A	0.2605	0.2432	0.3141	0.2700
NS 3-B	0.1881	0.1725	0.3658	0.2352
NS 4	0.2201	0.2004	0.3202	0.2950
NS 5	0.3630	0.3548	0.2711	0.3425
NS 6	N/A	N/A	N/A	N/A

predictor in the blind prediction phase. Figs. 36–41 show the RMSE values computed for types A, B, and C simulations of the centrifuge tests conducted at KU, CU, NCU, ZU, and UCD.

It is clear that once the predictors learned about the performance of their type A simulations (discussed in the LEAP-GWU workshop), they were able to effectively calibrate their models and submit significantly improved type C simulations. These simulations were also improved due to the use achieved base motions. It is also important to note that although the models were improved in the second round, the RMSE values for pore pressure records were only slightly improved. The RMSE values for accelerometer data were, however, substantially improved. The great improvement in RMSE values for acceleration is largely due to the use of the measured base input acceleration as opposed to the input acceleration. The lack of major improvement in the pore pressure predictions may indicate that the pore pressures predicted by the models were not especially sensitive to the differences in the input motions.

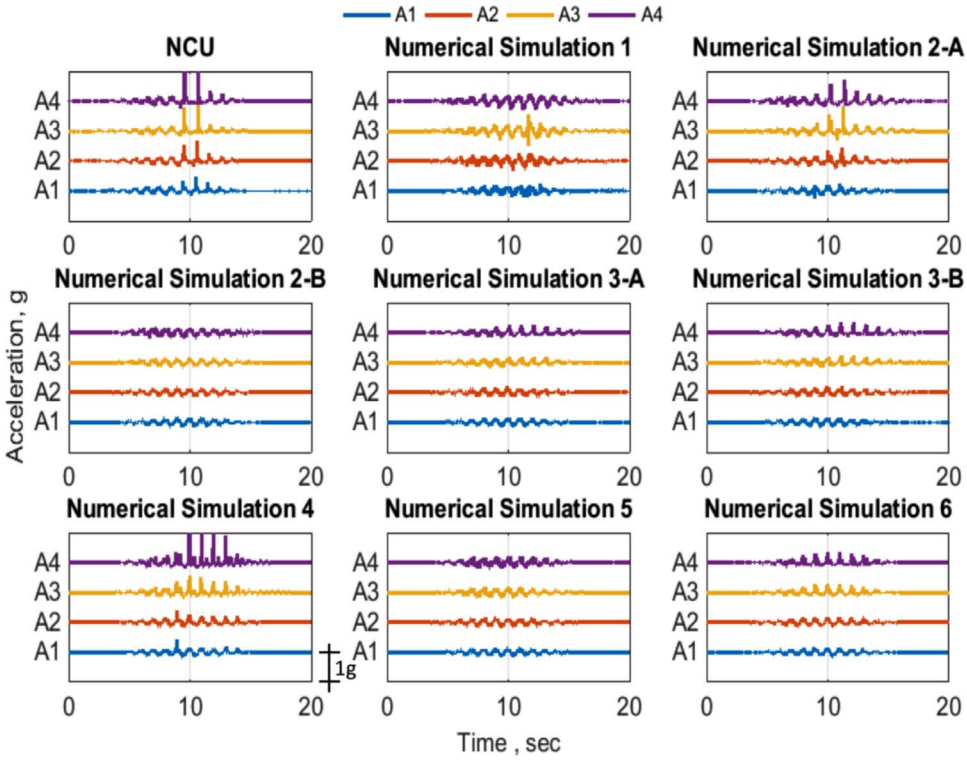

Fig. 26. Comparison of type C simulations of acceleration time histories computed at the location of A1 to A4 with the Results of the NCU Test, Motion #2 (see Fig. 1 for transducer locations.).

RMSE

	A1	A2	A3	A4
NS 1	0.0562	0.0974	0.1643	0.2500
NS 2-A	0.0266	0.0567	0.0985	0.1580
NS 2-B	0.0654	0.1212	0.1960	0.2703
NS 3-A	0.0672	0.1194	0.1840	0.2557
NS 3-B	0.0674	0.1088	0.1743	0.2357
NS 4	0.0393	0.0630	0.1242	0.2146
NS 5	0.0675	0.1184	0.1793	0.2482
NS 6	0.0678	0.1121	0.1637	0.2357

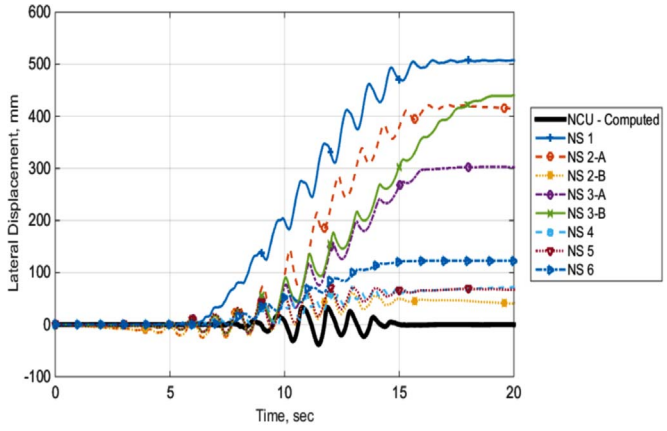

Fig. 27. Comparison of the type C simulations of lateral displacement time histories with the results of the NCU Test, Motion #2 (see Fig. 1 for transducer locations.).

6. Concluding remarks

Three different types of validation exercises have been presented in this paper. One is a True Prediction (TP) for which the prediction is submitted prior to the experiment being conducted. In this case, the quality of prediction depends on the validity of the numerical model and the accuracy with which the experiment followed the specifications. Due to the complexity of shakers on centrifuges and many variables in the experiments, differences between experimental results are inevitable. The second type of validation exercise has been called type B simulations, which is superior to type A simulation in some respects. Substantial discrepancies between specified and actual boundary conditions (e.g., ground motions) and initial conditions (density, geometry, and sensor locations) can be accounted for in type B simulations. A main criticism of validation by type B simulation is that it opens a possibility of unintentional leaking of results or hints. The third type of validation exercise has been called type C simulations. For type C, the simulation is done after the modeler has seen and studied the

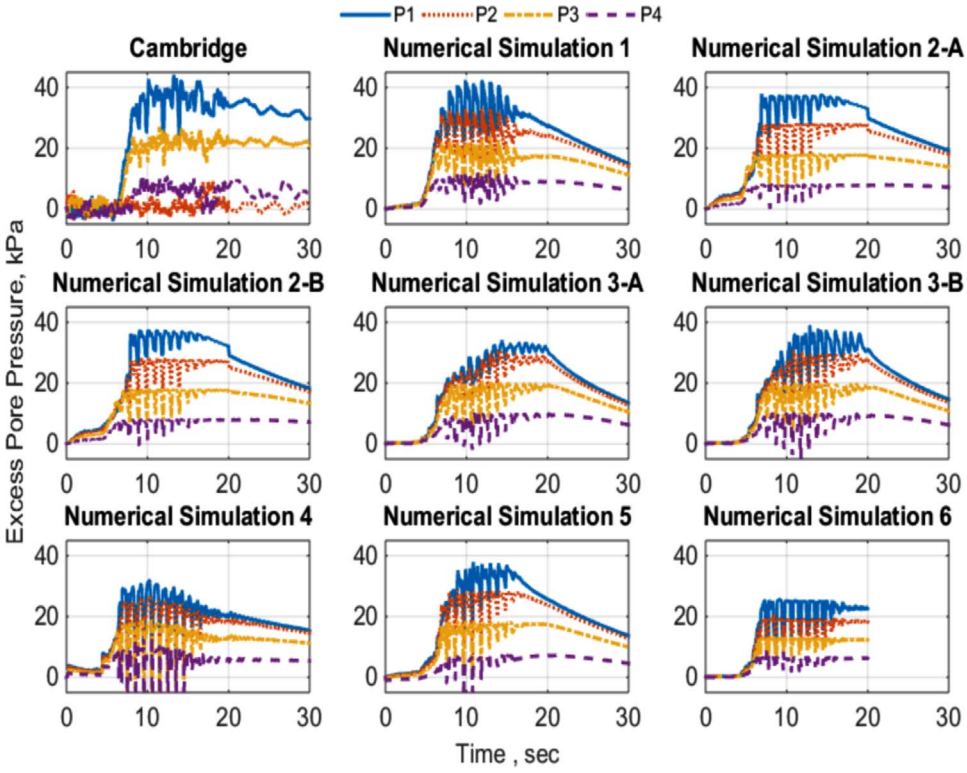

Fig. 28. Comparison of type C simulations of excess pore water pressure time histories computed at the Location of P1, P2, P3, and P4 with the Results of the Cambridge University (CU) Test, Motion #2 (see Fig. 1 for transducer locations.).

RMSE-t16

	P1	P2	P3	P4
NS 1	0.2213	0.6507	0.3562	0.4095
NS 2-A	0.1950	0.6614	0.3428	0.3648
NS 2-B	0.1267	0.6237	0.3074	0.3345
NS 3-A	0.2050	0.5680	0.2924	0.3263
NS 3-B	0.1822	0.5880	0.3075	0.3588
NS 4	0.3017	0.5255	0.4262	0.4888
NS 5	0.1590	0.6043	0.3006	0.2678
NS 6	0.2830	0.4452	0.3866	0.2912

RMSE-t30

	P1	P2	P3	P4
NS 1	0.2496	0.6513	0.3590	0.3872
NS 2-A	0.1965	0.6961	0.3299	0.3427
NS 2-B	0.1754	0.6674	0.3170	0.3265
NS 3-A	0.2459	0.6259	0.3209	0.3569
NS 3-B	0.2266	0.6379	0.3290	0.3594
NS 4	0.3401	0.5267	0.4629	0.3931
NS 5	0.2445	0.6185	0.3527	0.2602
NS 6	N/A	N/A	N/A	N/A

experimental results. The modeler may or may not spend a lot of effort in trial and error calibration of parameters to fit the results. Type C simulations can provide validation that a numerical model is able to predict an experimental result, but it cannot provide validation of the ability of a modeler ability to select numerical model parameters. Type C simulation can be a difficult test of a numerical simulation platform, especially if the time series of results (including frequency content, phase, and residual displacements) of the simulation and experiment are compared for many sensor types and sensor locations. For example the results presented in this paper showed that significant RMSE (root mean squared error) was observed for all numerical models during type C simulation exercise.

Detailed comparisons are presented for LEAP-GWU-2015: type A simulations of Motion #2, type B simulation of Motion #4, and type C simulation of Motion#2. These comparisons show that a sub-set of type A simulations were good in agreement with the responses measured in

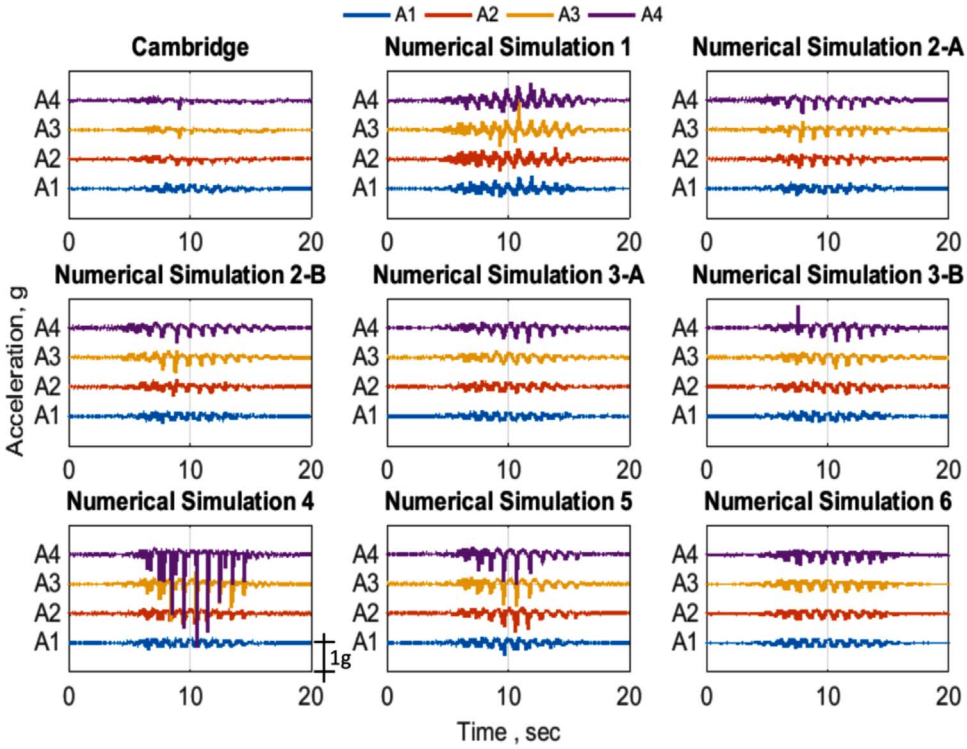

Fig. 29. Comparison of type C simulations of acceleration time histories computed at the location of A1 to A4 with the results of the Cambridge University (CU) Test, Motion #2 (see Fig. 1 for transducer locations.).

RMSE

	A1	A2	A3	A4
NS 1	0.0959	0.1938	0.2836	0.2951
NS 2-A	0.0455	0.0791	0.1165	0.1636
NS 2-B	0.0347	0.0731	0.1440	0.1986
NS 3-A	0.0366	0.0900	0.1495	0.1789
NS 3-B	0.0369	0.0919	0.1483	0.1829
NS 4	0.0570	0.1334	0.3043	0.5739
NS 5	0.0584	0.1641	0.2516	0.2809
NS 6	0.0417	0.1048	0.1527	0.1676

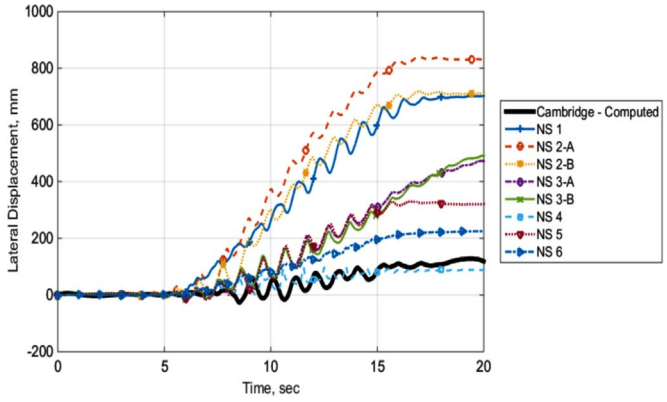

Fig. 30. Comparison of the type C simulations of lateral displacement time histories with the results of the Cambridge University (CU) Test, Motion #2 (see Fig. 1 for transducer locations.).

the centrifuge experiments. It is also observed that learning from the comparisons of their type A simulations with the measured responses, the predictors were able to significantly improve their simulations of a subsequent event (Motion #4, PGA = 0.25*g*) in which the same soil specimen was subjected to a larger base excitation (type B simulations). Moreover, the type C simulations show very good agreement with the experimental results obtained for the smaller base excitation (Motion #2, PGA = 0.15*g*) that was used in the true prediction exercise. This appears to be partly due to the adjustment of the constitutive model parameters and partly due to the selection of revised parameters for hydraulic conductivity of the soil.

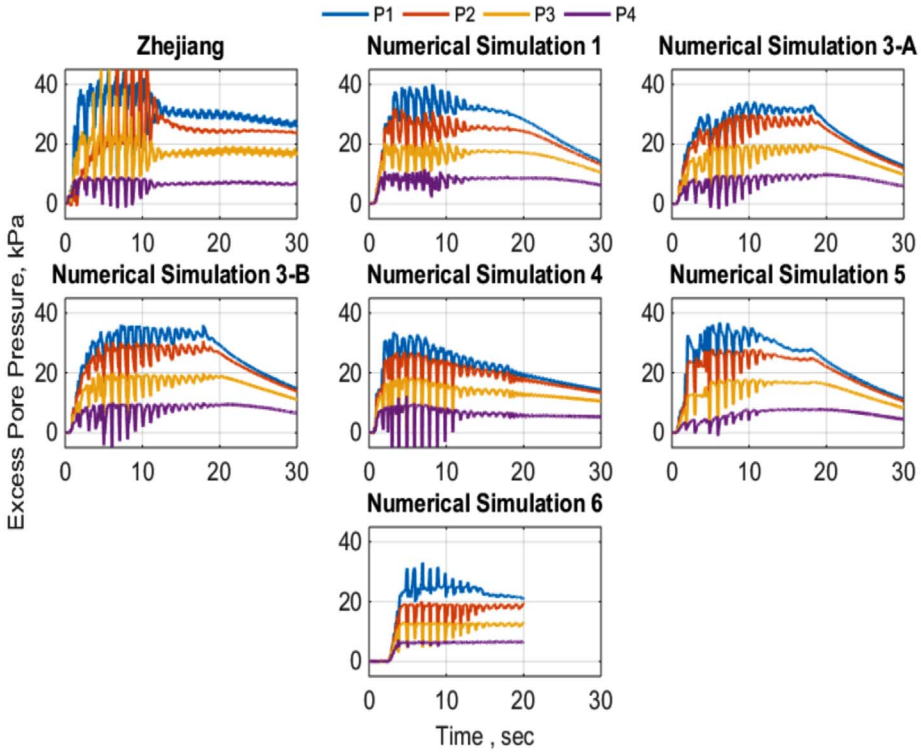

Fig. 31. Comparison of type C simulations of excess pore water pressure time histories computed at the Location of P1, P2, P3, and P4 with the Results of the Zhejiang University (ZU) Test, Motion #2 (see Fig. 1 for transducer locations.).

RMSE-t16

	P1	P2	P3	P4
NS 1	0.1560	0.3184	0.2496	0.2757
NS 3-A	0.2201	0.2603	0.3092	0.3613
NS 3-B	0.1935	0.2720	0.3066	0.3830
NS 4	0.2286	0.4007	0.3140	0.3225
NS 5	0.1725	0.2921	0.3118	0.3220
NS 6	0.3658	0.3912	0.4817	0.3190

RMSE-t30

	P1	P2	P3	P4
NS 1	0.1630	0.2622	0.2115	0.2208
NS 3-A	0.2150	0.2395	0.2562	0.2934
NS 3-B	0.1840	0.2317	0.2440	0.3055
NS 4	0.2523	0.3459	0.2947	0.2534
NS 5	0.2125	0.2754	0.2827	0.2450
NS 6	N/A	N/A	N/A	N/A

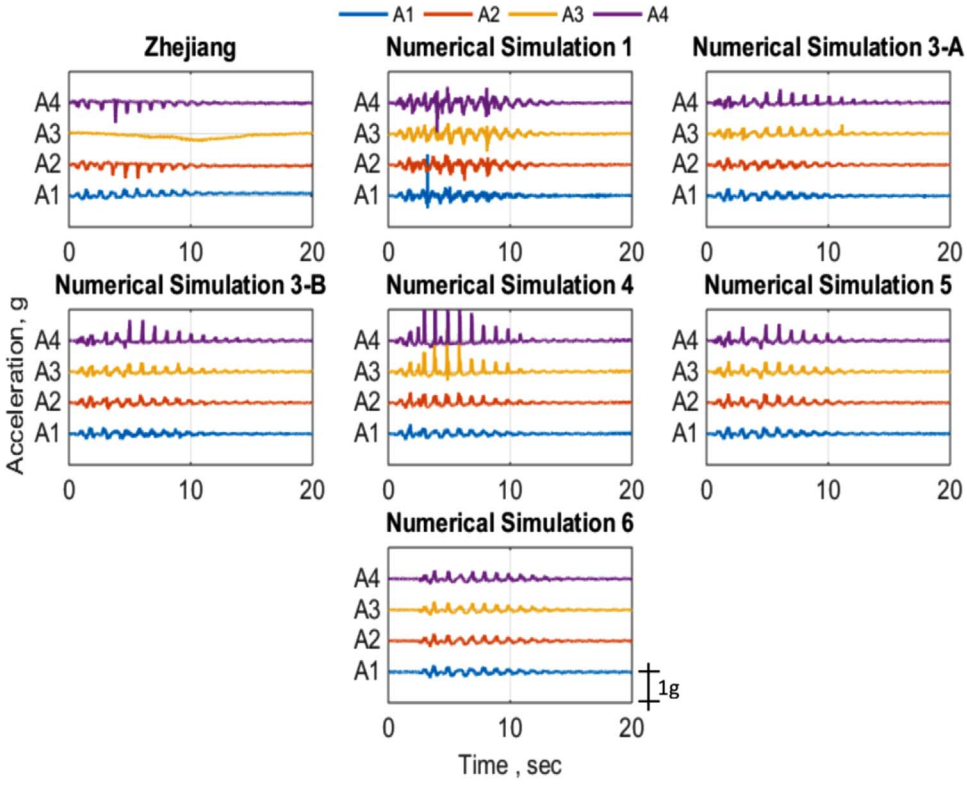

Fig. 32. Comparison of type C simulations of acceleration time histories computed at the location of A1 to A4 with the Results of the Zhejiang University (ZU) Test, Motion #2 (see Fig. 1 for transducer locations.).

RMSE

	A1	A2	A3	A4
NS 1	0.1048	0.1219	0.3331	0.1864
NS 3-A	0.0646	0.1467	0.2286	0.1140
NS 3-B	0.0595	0.1412	0.2347	0.0794
NS 4	0.0567	0.1104	0.4023	0.3986
NS 5	0.0576	0.1237	0.2593	0.1026
NS 6	0.0521	0.1461	0.2338	0.1549

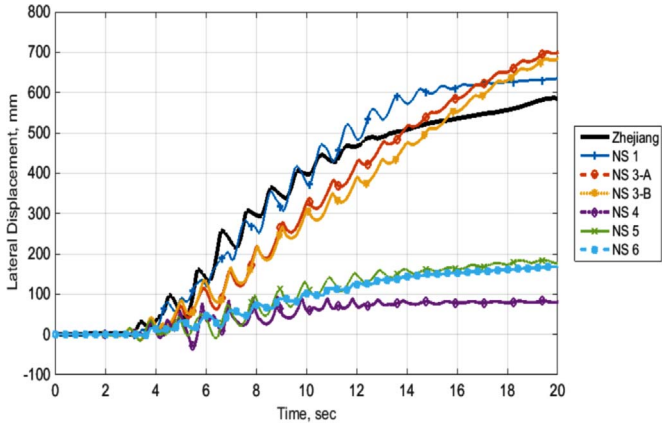

Fig. 33. Comparison of the predicted lateral displacement time histories with the results of the Zhejiang University (ZU) Test, Motion #2 (see Fig. 1 for transducer locations.).

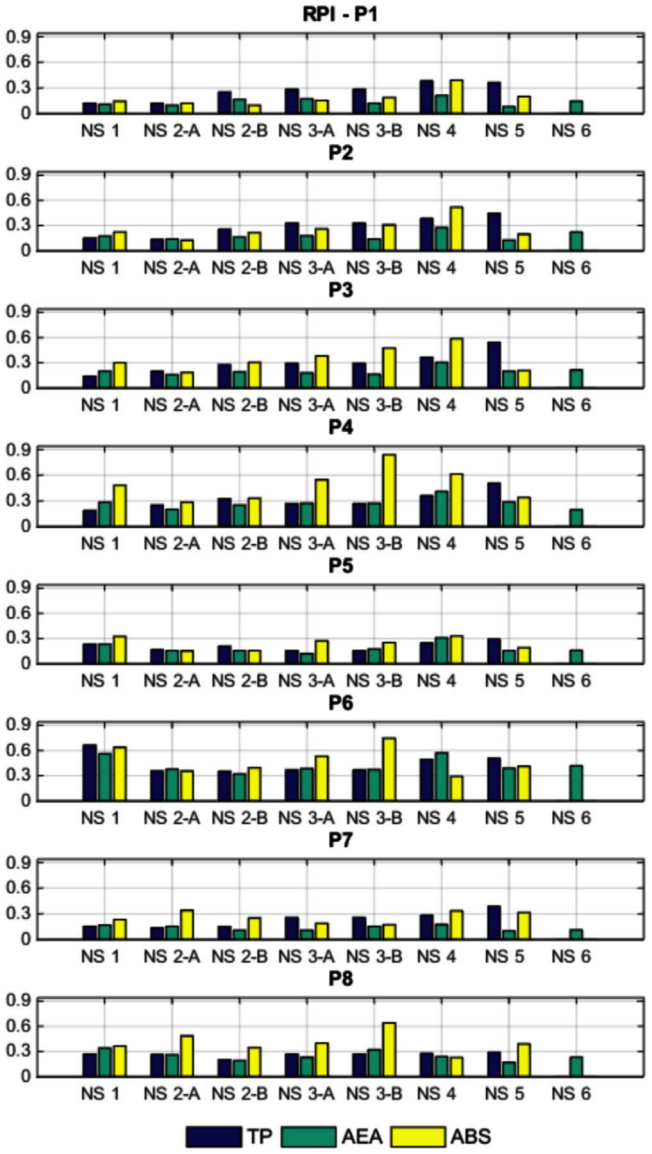

Fig. 34. Summary of RMSE for the numerical simulations of the RPI centrifuge test; pore water pressure time histories.

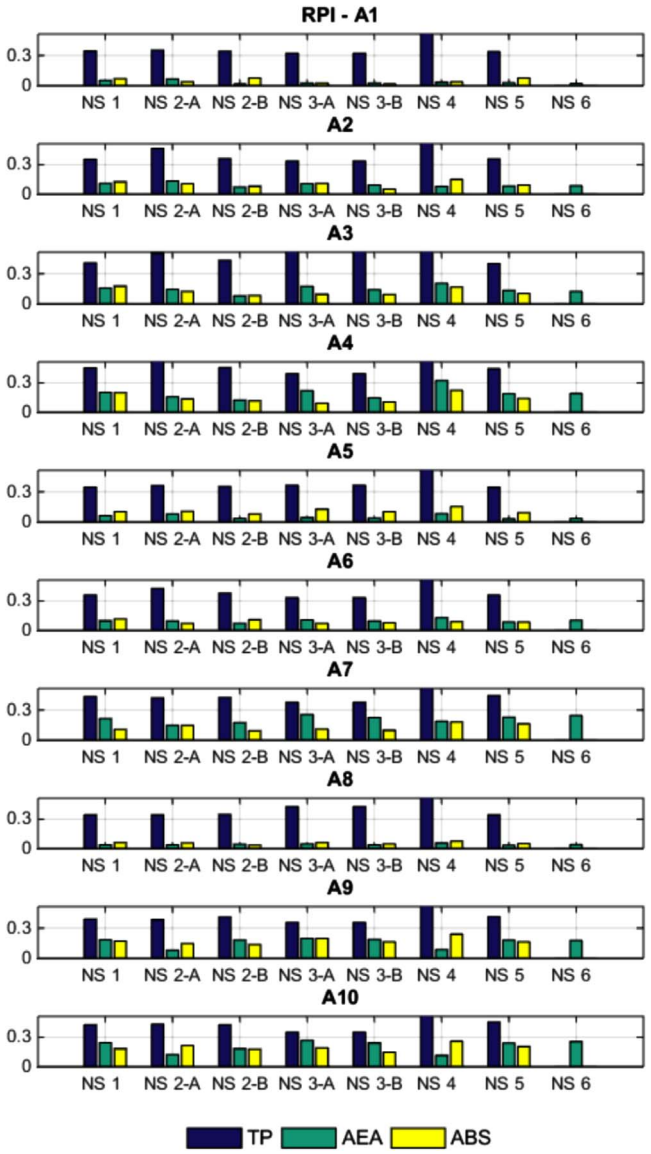

Fig. 35. Summary of RMSE values for the numerical simulations of the RPI centrifuge test; acceleration time histories.

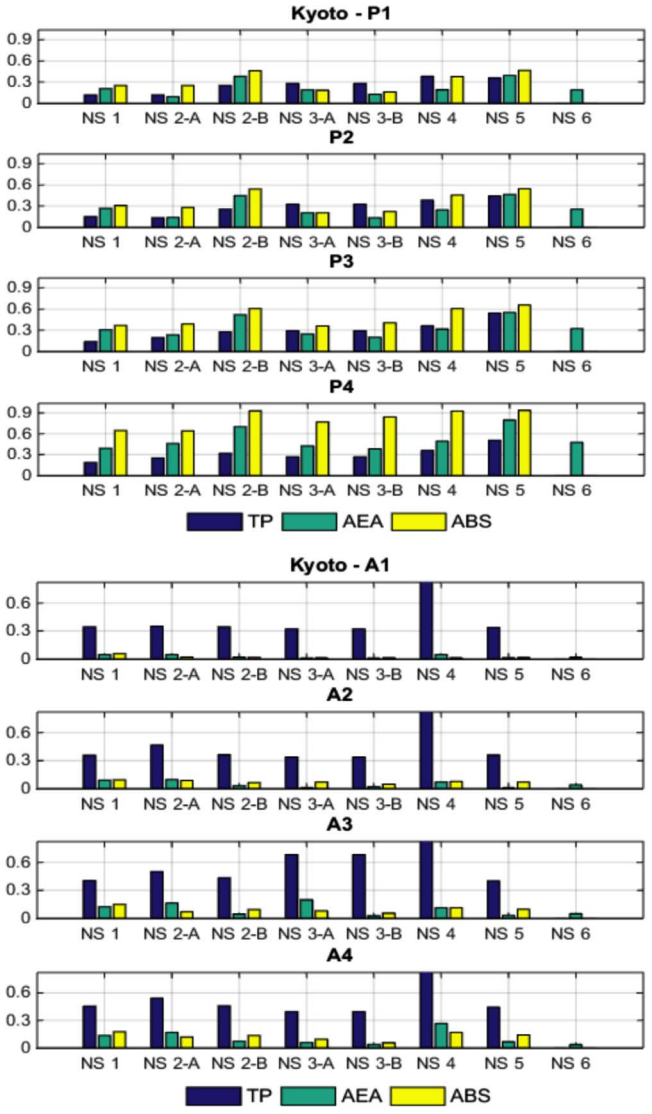

Fig. 36. Summary of RMSE values for the numerical simulations of the KU centrifuge test.

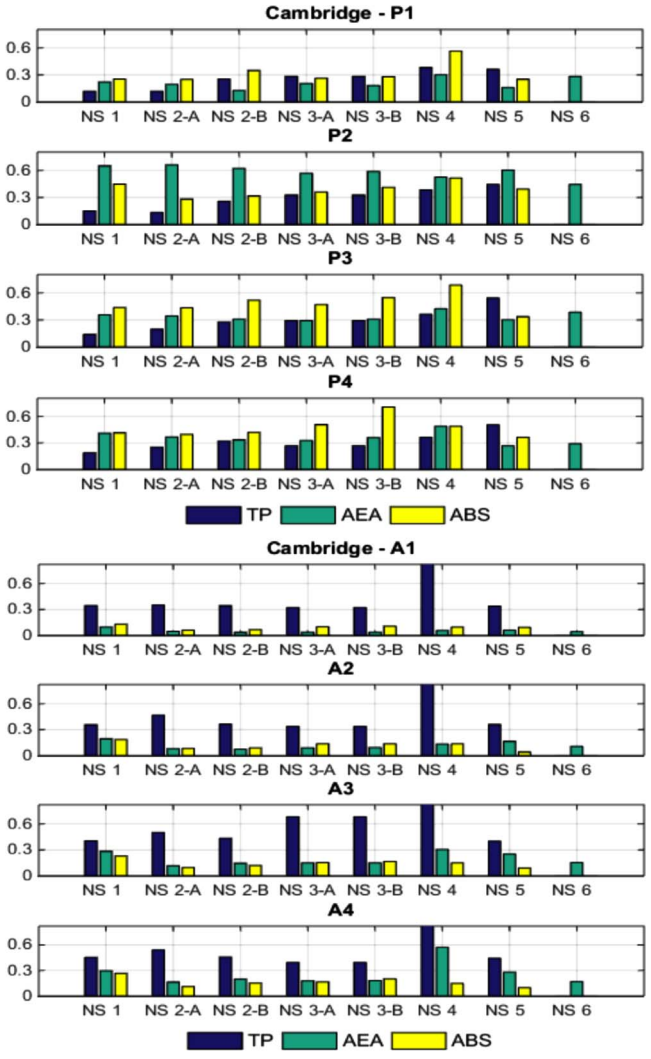

Fig. 37. Summary of RMSE values for the numerical simulations of the CU centrifuge test.

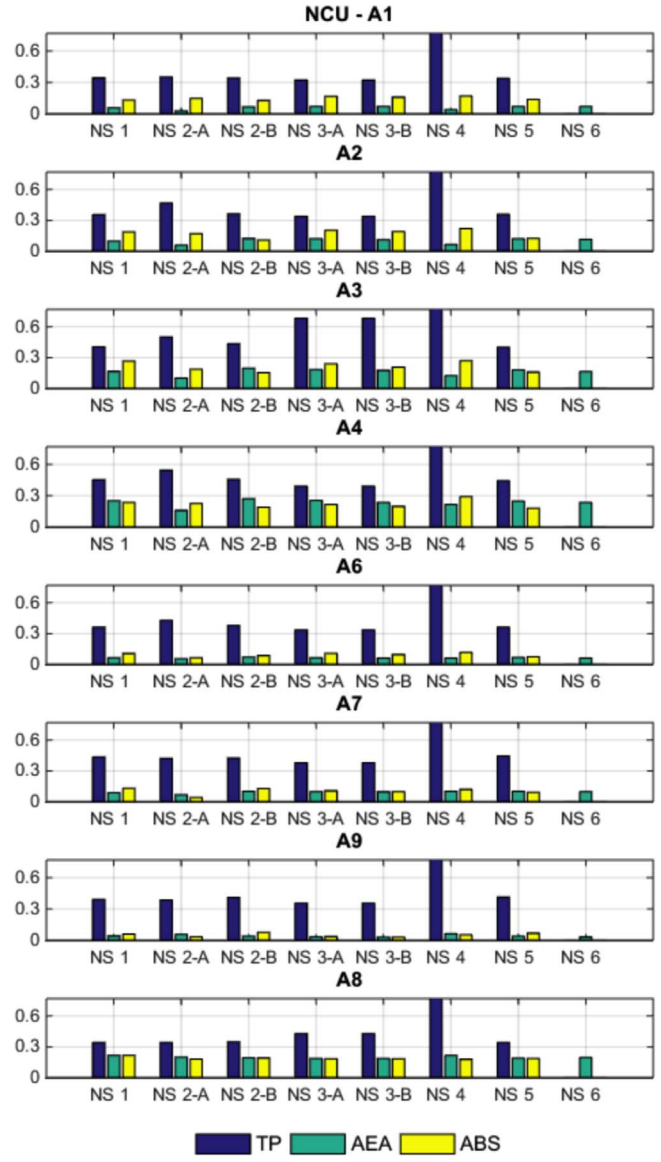

Fig. 38. Summary of RMSE for the numerical simulations of the NCU centrifuge test; pore water pressure time histories.

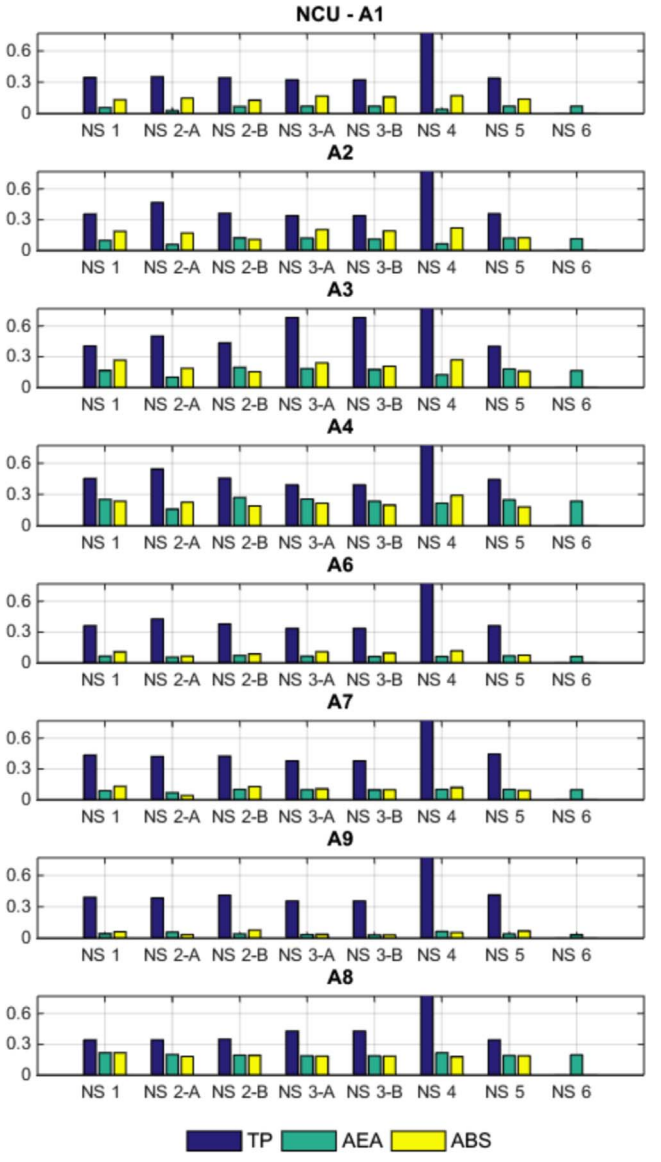

Fig. 39. Summary of RMSE values for the numerical simulations of the NCU centrifuge test; acceleration time histories.

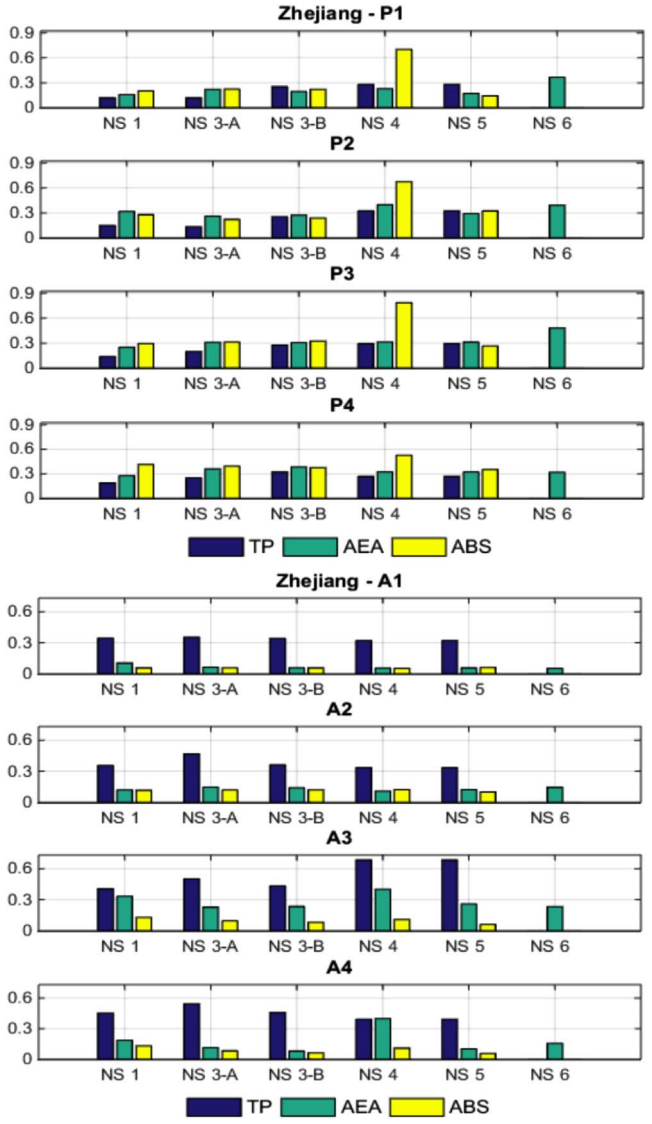

Fig. 40. Summary of RMSE values for the numerical simulations of the ZU centrifuge test.

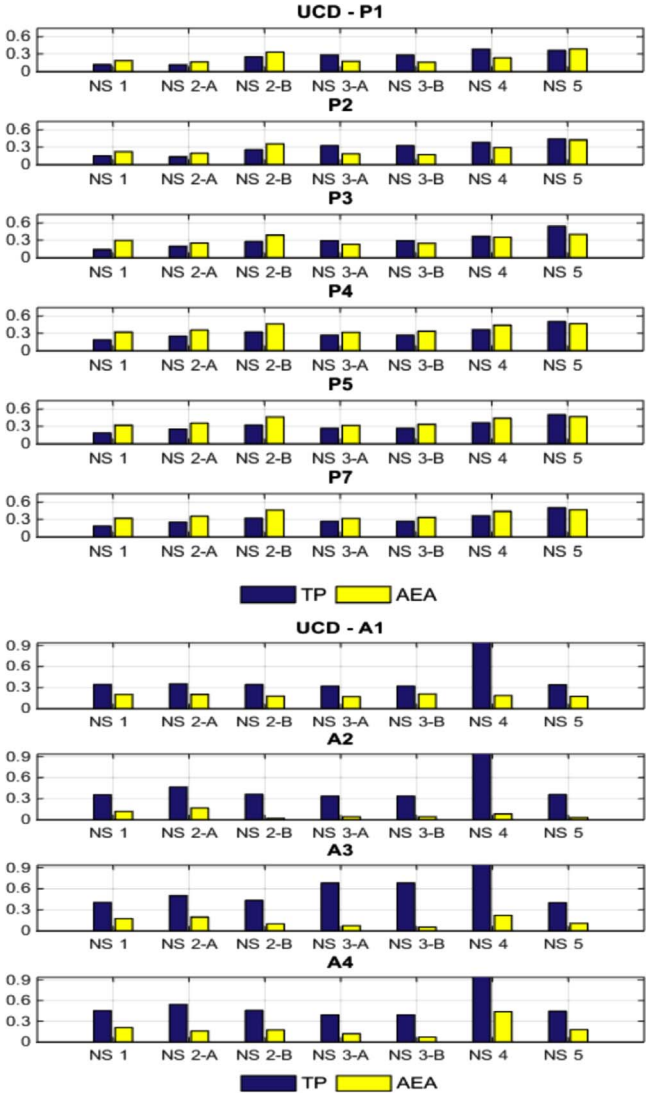

Fig. 41. Summary of RMSE for the numerical simulations of the UCD centrifuge test.

Acknowledgment

The planning phase of the LEAP project has been funded by the US National Science Foundation NEES research program directed by Dr. Richard Fragaszy, through the Grants CMMI-1344705, CMMI-1344630, and CMMI-1344619 to the George Washington University, the University of California Davis, and the Rensselaer Polytechnic Institute, respectively. This support is gratefully acknowledged. The work of Zhejiang University team has been funded by the National Natural Science Foundation of China (No. 51578501), the National Program for Special Support of Top-Notch Young Professionals (2013), the Zhejiang Provincial Natural Science Foundation of China (No. LR15E080001) and the National Basic Research Program of China (973 Project) (No. 2014CB047005).

Appendix A. Supplementary material

Supplementary data associated with this article can be found in the online version at http://dx.doi.org/10.1016/j.soildyn.2017.05.015.

References

[1] Abdoun T, El-Sekelly W, Dobry R, Thevanayagam S, Gonzalez M. CENSEIS: centrifuge and full-scale modeling of seismic pore pressures in sands; 2014. ⟨https://nees.org/resources/13418⟩.

[2] Allmond J, Kutter BL, Bray J, Hayden C. FLIQ: foundation and ground performance in liquefaction experiments. Netw Earthq Eng Simul (NEES) 2014. http://dx.doi.org/10.4231/D3M61BQ73.

[3] Armstrong RJ. Numerical analysis of LEAP centrifuge experiments using a practice-based approach. J Soil Dyn Earthq Eng 2017 [Submitted for publication, Special Issue on LEAP-2015].

[4] Arulanandan K, Scott RF . Verification of numerical procedures for the analysis of soil liquefaction problems. In: Proceedings of the international conference on the verification of numerical procedures for the analysis of soil liquefaction problems. Vols. 1 and 2. Rotterdam (The Netherlands): A. A. Balkema; 1993–1994.

[5] Beaty MH. Application of UBCSAND to the LEAP centrifuge experiments. J Soil Dyn Earthq Eng 2017 [Submitted for publication, Special Issue on LEAP-2015].

[6] Bilotta E, Lanzano G, Madabhushi SPG, Silvestri F. A round robin on tunnels under seismic actions. Acta Geotech 2014;9(4):563–79.

[7] Brinkgreve RBJ, Engin E, Swolfs WM. PLAXIS, finite element code for soil and rock analysis, user's manual; 2012. ⟨http://www.plaxis.nl/files/files/2D-0-Gen-Info_02.pdf⟩.

[8] Byrne PM. A cyclic shear-volume coupling and pore-pressure model for sand. In: Proceedings of the second international conference on recent advances in geotechnical earthquake engineering and soil dynamics. St. Louis, Paper no. 1.24; 1991. p. 47–55.

[9] Byrne PM, Park SS, Beaty M. Seismic liquefaction: centrifuge and numerical modeling. In: Proceedings of the 3rd international FLAC symposium. Sudbury (Canada); 2003.
[10] Byrne PM, Park SS, Beaty ML, Sharp MK, Gonzalez L, Abdoun T. Numerical modeling of liquefaction and comparison with centrifuge tests. Can Geotech J 2004;41(2):193–211.
[11] Boulanger RW, Ziotopoulou K. Formulation of a sand plasticity plane-strain model for earthquake engineering applications. J Soil Dyn Earthq Eng 2013;53:254–67. http://dx.doi.org/10.1016/j.soildyn.2013.07.006.
[12] Boulanger RW, Ziotopoulou K. PM4Sand (Version 3): a sand plasticity model for earthquake engineering applications. Report No. UCD/CGM-15/01. Davis (CA): Center for Geotechnical Modeling, University of California; 2015. p. 112.
[13] Carey TJ, Kutter BL, Manzari MT, Zegha, M. LEAP centrifuge test and numerical simulation specifications; 2015. ⟨https://nees.org/resources/13507⟩. ⟨http://doi.org/10.17603/DS2159T⟩.
[14] Carey TJ, Kutter BL, Manzari MT, Zeghal M, Vasko A. LEAP soil properties and element test data; 2015. ⟨https://nees.org/resources/13689⟩. ⟨http://doi.org/10.17603/DS2WC7W⟩.
[15] Carey TJ, Hashimoto C, Cimini D, Kutter BL. LEAP-GWU-2015 centrifuge test at UC Davis. J Soil Dyn Earthq Eng 2017 [In press, Special Issue on LEAP-2015].
[16] Cubrinovski M, Ishihara K. State concept and modified elastoplasticity for sand modeling. Soils Found 1998;38(4):213–25.
[17] Dafalias YF, Manzari MT. Simple plasticity sand model accounting for fabric change effects. ASCE J Eng Mech 2004;130(6):622–34.
[18] Dawson EM, Roth WH, Nesarajah S, Bureau G, Davis CA. A practice-oriented pore pressure generation model. In: Proceedings of the 2nd international FLAC; 2001.
[19] Elgamal A-W, Zeghal M, Parra E, Gunturi R. Identification and modeling of earthquake ground response, I: site amplification. Soil Dyn Earthq Eng 1996;15(8):499–522.
[20] Elgamal A, Yang Z, Parra E, Ragheb A. Modeling of cyclic mobility in saturated cohesionless soils. Int J Plast 2003;19(6):883–905.
[21] El-Shafee O, Spari M, Abdoun T, Zeghal M. Analysis of the response of a centrifuge model of a level site subjected to biaxial base excitation. Geo-Congress 2014 Technical Papers: Geo-Characterization and Modeling for Sustainability – Proceedings of the 2014 Congress. Geotechnical Special Publication, n 234 GSP; 2014. p 1081–90.
[22] El Shamy U, Zeghal M, Dobry R, Thevanayagam S, Elgamal A, Abdoun T, et al. Micromechanical aspects of earthquake-induced lateral spreading. ASCE Int J Geomech 2010;10:190.
[23] Finn WD Liam, Yogendrakumar M, Yoshida N, Yoshida H. TARA-3: a program to compute the response of 2-D embankments and soil-structure interaction systems to seismic loadings. Vancouver, Canada: University of British Columbia, Department of Civil Engineering; 1986.
[24] Ghofrani A, Arduino P. Prediction of LEAP centrifuge test results using a pressure-dependent bounding surface constitutive model. J Soil Dyn Earthq Eng 2017 [In press, Special Issue on LEAP-2015].
[25] Hung WY, Lee CJ, Hu L-M. Study of the effects of container boundary and slope dip on soil liquefaction by centrifuge modeling. J Soil Dyn Earthq Eng 2017 [Submitted for publication, Special Issue on LEAP-2015].
[26] Iai S, Matsunaga Y, Kameoka T. Strain space plasticity model for cyclic mobility. Soils Found 1992;32(2):1–15.
[27] Iai S, Tobita T, Ozutsumi O, Ueda K. Dilatancy of granular materials in a strain space multiple mechanism model. Int J Numer Anal Methods Geomech 2011;35(3):360–92.
[28] Iai S, Ueda K, Tobita T, Ozutsumi O. Finite strain formulation of a strain space multiple mechanism model for granular materials. Int J Numer Anal Methods Geomech 2013;37(9):1189–212.
[29] Ishihara K. Liquefaction and flow failure during earthquakes. Geotechnique 1993;43(3):351–415.
[30] Itasca Consulting Group Inc. Fast Langrangian analysis of Continua, FLAC-2D, version 8.0; 2016.
[31] Jeremic B, Cheng Z, Taiebat M, Dafalias YF. Numerical simulation of fully saturated porous materials. Int J Numer Anal Methods Geomech 2008;32(13):1635–60.
[32] Kokkali P, Abdoun T, Zeghal M. Physical modeling of soil liquefaction: overview of LEAP production test 1 at Rensselaer Polytechnic Institute. J Soil Dyn Earthq Eng 2017 [In press, Special issue on LEAP-2015].
[33] Kutter BL, Manzari MT, Zeghal M, Zhou YG, Armstrong RJ. Proposed outline for LEAP verification and validation processes. In: Proceedings of the fourth international conference on geotechnical engineering for disaster mitigation and rehabilitation. Kyoto (Japan); 2014.
[34] Kutter BL, Carey TJ, Hashimoto T, Manzari MT, Vasko A, Zeghal M, et al.. LEAP Databases for verification, validation, and calibration of codes for simulation of liquefaction. In: Proceedings of the 6th international conference on earthquake geotechnical engineering. Christchurch (New Zealand); 2015.
[35] Kutter BL, Carey TJ, Hashimoto T, Zeghal M, Abdoun T, Kokkali P, et al. LEAP-GWU-2015 experiment specifications, results, and comparisons. J Soil Dyn Earthq Eng 2017 [Submitted for publication, special issue on LEAP-2015].
[36] Ling HI, Yang S. A unified sand model based on critical state and generalized plasticity. J Eng Mech ASCE 2006;132:1380–91.
[37] Madabhushi SSC, Haigh S, Madabhushi GSP. LEAP-GWU-2015: centrifuge and numerical modelling of slope liquefaction at the University of Cambridge. J Soil Dyn Earthq Eng 2017 [In press, special issue on LEAP-2015].
[38] Manzari MT, Dafalias YF. A critical state two-surface plasticity model for sands. Geotechnique 1997;49(2):252–72.
[39] Manzari MT. Application of micropolar plasticity to post-failure analysis in geomechanics problems. Int J Numer Anal Methods Geomech 2004;28(10):1011–32.
[40] Manzari MT, Kutter BL, Zeghal M, Iai S, Tobita T, Madabhushi SPG, Haigh SK, Mejia L, Gutierrez DA, Armstrong RJ, Sharp MK, Chen YM, Zhou YG. LEAP Projects: Concept and Challenges. In: Proceedings of the fourth international conference on geotechnical engineering for disaster mitigation and rehabilitation (4th GEDMAR). Kyoto, Japan; 2014.
[41] Manzari MT, Regueiro RA. Gradient plasticity modeling of geomaterials in a meshfree environment, Part I: theory and variational formulation. Int J Mech Res Commun 2005;32:36–546.
[42] Manzari MT. On Material versus structural response of saturated granular soils. In: Ling HI, Smyth A, Betti R (editors). Proceedings of the fourth biot conference on Poromechanics including the second Frank L. Dimaggio Symposium. Columbia University, DESTech Pub.; June 8–10, 2009. p. 1033–9.
[43] Manzari MT, Yonten KY. Analysis of geostructures using a two-scale constitutive model. In: Proceedings of the first international conference on advances in interaction and multiscale mechanics. South Korea; May 30 to June 3, 2010.
[44] Manzari MT, Yonten K. Comparison of two integration schemes for a micropolar plasticity model. Comput Methods Civil Eng 2011;2(2011):21–42.
[45] Manzari MT, Yonten K. Analysis of post-failure response of sands using a critical state micropolar plasticity model. Interact Multiscale Mech 2011;4(3):187–206.
[46] Papadimitriou AG, Bouckovalas GD, Dafalias YF. Plasticity model for sand under small and large cyclic strains. J Geotech Geoenviron Eng 2001;127(11):973–83.
[47] Perlea VG, Beaty MH. Corps of Engineers' practice in the evaluation of seismic deformation of embankment dams. In: Proceedings of the fifth international conference on recent advances in geotechnical earthquake engineering and soil dynamics. San Diego: Special Lecture SPL-6; May 24–29, 2010. p. 1–30.
[48] Prevost JH. DYNAFLOW, Version 98, Release 02.A. Princeton, New Jersey: Princeton University, Department of Civil Engineering & Op. Res.; 1998.
[49] Regueiro RA, Borja RI. Plane strain finite element analysis of pressure sensitive plasticity with strong discontinuity. Int J Solids Struct 2001;38(21):3647–72.
[50] Taiebat M, Dafalias YF. SANISAND: simple anisotropic sand plasticity model. Int J Numer Anal Method Geomech 2008;32:915–48.
[51] Tobita T, Manzari MT, Ozutsumi O, Ueda K, Uzuoka R, Iai S. Benchmark centrifuge tests and analyses of liquefaction-induced lateral spreading during earthquake. In: Iai S, editor. Geotechnics for catastrophic flooding events. London: Taylor and Francis Group; 2014.
[52] Tobita T. Effect of the radial gravity field on dynamic response of saturated sloping grounds in centrifuge model testing. J Soil Dyn Earthq Eng 2017 [Submitted for publication, Special issue on LEAP-2015].
[53] Ueda K, Iai S. Numerical predictions for centrifuge model tests of a liquefiable sloping ground using a strain space multiple mechanism model based on the finite strain theory. J Soil Dyn Earthq Eng 2017 [Submitted for publication, Special issue on LEAP-2015].
[54] Vasko A. Master's thesis submitted to the Department of Civil and Environmental Engineering at the George Washington University; 2015.
[55] Wang ZL, Dafalias YF, Shen CK. Bounding surface hypo-plasticity model for sands. J Eng Mech ASCE 1990;116(5):993–1001.
[56] Wang ZL, Makdisi FI. Implementing a bounding surface hypoplasticity model for sand into the FLAC program. In: FLAC and numerical modeling in geomechanics. Netherlands: A.A. Balkema; 1999. p. 483–90.
[57] Wang ZL, Makdisi FI, Egan J. Practical applications of a nonlinear approach to analysis of earthquake-induced liquefaction and deformation of earth structures. J Soil Dyn Earthq Eng 2006;26(2–4):231–52.
[58] Yang Z, Elgamal A, Parra E. A computational model for cyclic mobility and associated shear deformation. J Geotech Geoenviron Eng ASCE 2003;129(12):1119–27.
[59] Yang Z, Elgamal A. Multi-surface cyclic plasticity sand model with lode angle effect. J Geotech Geol Eng 2004;26(3):3350348.
[60] Yu H, Zeng X, Li B, Ming H. Effect of fabric anisotropy on liquefaction of sand. ASCE J Geotech Geoenviron Eng 2013;139(5):765–74.
[61] Zeghal M, El Shamy U. A continuum-discrete hydromechanical analysis of granular deposit liquefaction. Int J Numer Anal Meth Geomech 2004;28:1361–83.
[62] Zeghal M, Manzari MT, Kutter BL, Abdoun T. LEAP: Selected data for Class C calibrations and Class A Validations. In: Proceedings of the fourth international conference on geotechnical engineering for disaster mitigation and rehabilitation (4th GEDMAR); 2014.
[63] Zeghal M, Tsigginos C. A micromechanical analysis of the effect of fabric on low-strain stiffness of granular soils. Soil Dyn Earthq Eng 2015;70:153–65.
[64] Zeghal M, Manzari MT, Kutter BL, Abdoun T. LEAP: Data, calibration and validation of soil liquefaction odels. In: Proceedings of the 6th international conference on earthquake geotechnical engineering. Christchurch (New Zealand); 2015.
[65] Zeghal M, Goswami N, Kutter B, Manzari MT, Abdoun T, Arduino P, et al. Stress-strain response of the LEAP-2015 centrifuge tests and numerical predictions. J Soil Dyn Earthq Eng 2017 [Submitted for publication, Special issue on LEAP-2015].
[66] Zhou E, Sun Z-B, Chen Y-M. Zhejiang University benchmark Centrifuge test for LEAP-GWU-2015 and liquefaction responses of a sloping ground. J Soil Dyn Earthq Eng 2017 [In press, Special issue on LEAP-2015].
[67] Zienkiewicz OC, Chan AHC, Pastor M, Schrefler BA, Shiomi T. Computational geomechanics with special reference to earthquake engineering. England: John Wiley and Sons; 1998.
[68] Ziotopoulou K. Seismic response of liquefiable sloping ground: class A and C numerical predictions of centrifuge model responses. J Soil Dyn Earthq Eng 2017 [In press, Special issue on LEAP-2015].